www.sciencemag.org/cgi/content/full/science.1243192/DC1

Supplementary Materials for

Product-to-Parent Reversion of Trenbolone: Unrecognized Risks for Endocrine Disruption

Shen Qu, Edward P. Kolodziej,* Sarah A. Long, James B. Gloer, Eric V. Patterson, Jonas Baltrusaitis, Gerrad D. Jones, Peter V. Benchetler, Emily A. Cole, Kaitlin C. Kimbrough, Matthew D. Tarnoff, David M. Cwiertny*

*Corresponding author. E-mail: koloj@unr.edu (E.P.K.); david-cwiertny@uiowa.edu (D.M.C.)

Published 26 September 2013 on *Science* Express
DOI: 10.1126/science.1243192

This PDF file includes:

Other Supplementary Material for this manuscript includes the following:
(available at www.sciencemag.org/cgi/content/full/science.1243192/DC1)

Materials and Methods

Reagents

A complete reagents list is available in our earlier works (*14, 15*). All TBA metabolites were acquired from commercial suppliers, with high purity 17β-trenbolone (17β-TBOH; Steraloids; > 99%), 17α-trenbolone (17α-TBOH; Cerilliant; 99%), trendione (TBO; Steraloids; >99%), and dienogest (Selleck Chemicals; >99%) used as received. Dienedione was acquired from an online vendor and its purity and structure were confirmed via NMR.

Light source and photoreactor details.

Most laboratory experiments used a commercially available 450 W Xenon arc lamp (Newport Corporation) and a water-jacketed borosilicate photoreactor described previously (*14*). Where indicated, a small number of experiments requiring larger sample volumes utilized a Suntest CPS+ solar simulator. A limited number of experiments (detailed below) also utilized natural sunlight.

Stability of TBA Metabolites and Photoproduct Mixtures.

A variety of experimental systems were utilized to assess photoproduct stability. Experiments generally involved a period in which a solution of TBA metabolite was irradiated via simulated sunlight followed by a period in which the resulting photoproduct mixture was stored in the absence of light under controlled temperature and pH. During the light and dark periods, the concentration of the parent TBA metabolite and photoproducts were monitored over time.

Day-Night Cycling of TBA Metabolites and their Photoproducts. To monitor the long-term stability of TBA metabolites and photoproducts, experiments simulated day-night cycling. Experiments were conducted at pH 7 (maintained with a 5 mM phosphate buffer) and 25°C (maintained with a recirculating water bath via the jacketed reactor) and an initial TBA metabolite concentration of 10 μM. The solution was irradiated with simulated sunlight for 12 h, during which samples were periodically withdrawn, transferred to a 2 mL amber autosampler vial, and analyzed immediately via HPLC with diode array detector (LC-DAD) with a typical analysis time of 10 minutes. After 12 h of irradiation, the photoreactor was removed from light and covered with aluminum foil for 12 h. During this dark period, samples were once again withdrawn periodically and analyzed immediately via LC-DAD according to the details referenced below in the Analytical Methods section. This sequence of light-dark sampling was conducted over a total of 72 h, simulating a three day period.

Long-Term Dark Stability of TBA Metabolite Photoproducts. Solutions of each TBA metabolite (10 μM) were photolyzed for 6 h at 25 °C and pH 7, resulting in >99% transformation based upon peak area loss during LC-DAD analysis. The photoreactor was then removed from light, covered with Al foil, and stored for up to one week (~150 h) at 25 °C.

Effect of Temperature on Photoproduct Stability. A 50-mL solution of 10 μM 17α-TBOH was prepared at pH 7 and photolyzed at 25°C to achieve ~99% transformation. The irradiated solution was then divided into four equal parts, each placed in a 40-mL amber bottle to avoid light. The four vials were then transferred either to a refrigerator (5°C) or a series of water baths (15, 25, and 35°C) for 6 days.

Effect of pH on Photoproduct Stability. Two protocols were followed to evaluate the influence of pH on photoproduct stability. First, a subset of photolysis experiments with each

TBA metabolite was conducted in DI water at 25°C. After 4-6 h of irradiation (resulting in ~99% transformation), metabolite solutions were divided into equal parts. One portion was adjusted to pH 2 with 5 M HCl while the other was adjusted to pH 12 with 5 M NaOH. Samples of the pH-adjusted solutions were then withdrawn and immediately analyzed by LC-DAD, and also by NMR in the case of 17β-TBOH.

The second approach involved conducting photolysis and subsequent dark stability experiments at different pH values (pH 5, 7, and 9) with 17α-TBOH at 25 °C. A 5 mM phosphate buffer was adjusted using 1 M HCl or 1 M NaOH to achieve pH values of 5 and 7, while a 5 mM borate buffer was used for pH 9. System pH was monitored over time and adjusted as needed to maintain the initial value (± 0.2 pH units). Photolysis experiments with 17α-TBOH (10 μM) were conducted over 6 h, after which the irradiated solution was transferred to a 40-mL amber vial and stored for up to 6 days at 25 °C.

Additional experiments explored the photolysis of TBO and subsequent (dark) photoproduct reversion at pH 5. These photolysis experiments were conducted utilizing solutions contained in 25-mL clear borosilicate glass vials. All samples consisted of 25 mL of distilled water with 5 mM phosphate buffer adjusted to pH 5 by 10 M HCl addition, analogous to photolysis experimental conditions described above. Samples contained 10 μM TBO and were placed in direct sunlight at 39°32'26.03"N, 119°48'46.91"W (Reno, Nevada) on May 24, 2013 for 7.5 hours centered around noon (1200). Control samples were wrapped in foil and placed in direct sunlight, then stored; notably, TBO was stable in these controls. After irradiation, samples were stored in the dark at 20 °C. At subsequent time periods, 2.0-mL aliquots of irradiated sample or controls were collected and transferred to 2.5-mL autosampler vials for immediate analysis via LC-DAD or LC-HRMS/MS analysis.

Reversion Experiments in More Complex Aquatic Matrices. Photolysis and dark regrowth experiments were conducted in more complex aquatic matrices representative of agriculturally impacted surface waters. These included solutions of our standard 5 mM phosphate buffer (pH 7) to which either 10 mg/L of Fluka Humic Acid (FHA; a model form of natural organic matter) or 5 mM sodium bicarbonate ($NaHCO_3$; or 250 mg/L as $CaCO_3$) was added. We note that additional experiments were conducted in 5 mM bicarbonate solution (pH 7) without phosphate buffer, and identical results were observed. Following our standard photolysis procedures, 10 μM of 17α-TBOH was photolyzed for 4 h in these solutions, after which the resulting product mixtures were stored in the dark for up to 100 h to monitor reversion.

Additional experiments with 17α-TBOH were conducted in samples of raw (unprocessed) Iowa River water. The sample was collected at the intake of the University of Iowa (UI) Water Treatment Plant (WTP), which treats Iowa River water for use on the UI campus. Characterization performed by the UI WTP revealed the following water quality parameters: turbidity: 15.1 NTU; alkalinity: 196 mg/L as $CaCO_3$; total hardness: 270 mg/L as $CaCO_3$; total dissolved organic carbon: 16.6 mg/L; pH: 8.2. As with systems with FHA and bicarbonate, 10 μM of 17α-TBOH was spiked into this water sample. The mixture was then photolyzed for 4 h, after which the resulting product mixture was stored in the dark for up to 100 h to monitor reversion. Controls were conducted to monitor the stability of 17α-TBOH in Iowa River water in the absence of light. These controls revealed no loss of 17α-TBOH over the timescales of our photolysis and reversion experiments.

Reversion Experiments using Environmentally Relevant Concentrations. Photolysis and dark stability experiments were also conducted with 17β-TBOH at a more environmentally relevant initial concentration (420 ng/L or 1.5 nM). Seven identical borosilicate beakers were

prepared with 100 mL of 420 ng/L 17β-TBOH in DI water. Each beaker was then photolyzed in parallel using a Suntest CPS+ solar simulator. Periodically, reactors were sacrificially sampled, in which the entire 100 mL volume was concentrated using a C18 cartridge. The cartridge was subsequently eluted with 0.5 mL of methanol, resulting in a 17β-TBOH concentration suitable for detection and analysis via LC-DAD.

Analytical Methods.

Details of all analytical methods are provided in our earlier publications (*14, 15*). Briefly, samples from laboratory photolysis experiments were analyzed primarily with an Agilent 1200 Series HPLC-DAD system. The method used an analytical wavelength of 350 nm for TBA metabolites and 254 nm for all photoproducts, a key diagnostic for distinguishing TBA metabolites with an intact trienone system from direct photolysis products lacking this structural feature (*15*). Products were further characterized using high resolution LC/MS/MS and/or NMR using methods and instrumentation described in our previous studies (*15*).

Theoretical Methods.

For TBO, computational chemical calculations were performed to assess the energetics of various transformation processes proposed herein. All structures were optimized using the M06-2X (*23*) density functional in combination with the 6-31+G(d,p) basis set. More accurate energies were obtained using the larger 6-311+G(2df,2p) basis set with the corresponding notation of M06-2X/6-311+G(2df,2p)//M06-2X/6-31+G(d,p). Gibbs free energy corrections obtained from M06-2X/6-31+G(d,p) Hessian calculations were used to correct the M06-2X/6-311+G(2df,2p) calculated energies. The SMD continuum solvation model (*24*) was used during geometry optimizations, Hessian calculations and single-point energy calculations to account for the effect of bulk aqueous solvation. Geometries were optimized without any constraints followed by vibrational frequency analysis. Absence of imaginary frequencies confirmed that all structures are minima on the potential energy surface. All reported energies are calculated Gibbs free energies at 298 K in 1 M aqueous solution, relative to Structure III (Figure S17). All calculations were performed using Gaussian 09 version B02 (*25*).

Field Photolysis Studies.

Studies were conducted to evaluate the occurrence and transformation of TBA metabolites under field conditions using a mesocosm system on a working rangeland (Sierra Foothills Research and Extension Center, Browns Valley, CA, NAD 83 UTM 104344915N; 645022E). To simulate a sunlit surface water containing typical agricultural runoff in a rangeland setting, a shallow collection pond (~400 L, <40 cm in maximum depth) was excavated in a low lying area that naturally accumulated water. After excavation, the pond was left undisturbed for 3 weeks to facilitate flushing of unconsolidated sediments and hydraulic stabilization. On December 9, 2012, 35 L of homogenized, fresh (< 2 days old) manure from four second-year heifers implanted with a low dose of TBA (Revalor G, Intervet/Merck Animal Health, 40 mg TBA, 8 mg estradiol) was placed into the pond with minimal disturbance after sundown (2200). This night time dose was designed to allow a dark period that would facilitate leaching of TBA metabolites from the animal wastes into the overlying shallow water, which initially contained no detectable TBA metabolites (a result confirmed by analysis of background samples; see Table S7). At periodic intervals (0600, 0900, 1100, and 1300 of the following day), 1-L samples were collected and pressure filtered (0.7-μm AP40 filters, Millipore, Billerica, MA) for triplicate

analysis of steroids by GC/MS/MS using previously published protocols (*26, 27*). The pond received full sunlight throughout the day (i.e., 0800-1500), and temperature and pH were also monitored in the pond throughout the experiment. Samples were spiked with d_3-17β-TBOH (100 ng/L) and extracted using 6 mL C-18 solid phase extraction cartridges (SPE, Restek, Bellefonte, PA) in the shade to prevent further phototransformation. At 1500 (sundown), we collected a 31-L sample (called the "baseline" sample) for subsequent analysis, which was immediately filtered and placed on ice for transport to the laboratory. Also in the field, we acidified three 1-L subsamples with sulfuric acid to pH=2.45 to investigate the impact of acidification on measured TBA metabolite concentrations arising from photoproduct reversion.

Upon arrival in the laboratory, the acidified sample was extracted, along with three 1-L aliquots of the baseline sample. We then investigated the effect of storage temperature and sample handling conditions by dividing the remaining baseline sample and placing 12 L into an incubator (35 °C "warm" samples) or a refrigerator (1 °C, "cold" samples). 1-L samples in triplicate were subsequently collected and immediately extracted from the incubator at 3, 6, 12, and 24 hours of storage, and from the refrigerator 12 and 24 hours after cooling. After 24 hours of storage in the refrigerator, the remaining 6 L of the baseline sample was transferred to the incubator and slowly warmed to 35 °C ("cold-to-warm" sample), and after an additional 12 and 24 hours of storage, triplicate 1-L samples were extracted.

SPE cartridges were eluted with 9 mL of methanol and water (95:5 v/v). The eluent was dried, resuspended (95:5 v/v dichloromethane/methanol), and passed through 6-mL Florisil cartridges (Restek) to reduce organic matrix interference. Next, the extracts were dried with nitrogen gas, derivatized using 50 μL of MSTFA-I_2 (1.4 mg I_2/mL MSTFA), immediately dried again to remove residual iodine, resuspended in 100 μL of MSTFA, heated to 60 °C (40 min.), and transferred to GC vials for analysis (*26*).

Supplementary Text

Identification of 5-hydroxy-17α-TBOH as a Phototransformation Product of 17α-TBOH.

Previously, we identified 12-hydroxy-17α-TBOH as the major photoproduct of 17α-TBOH in H_2O at pH 7 (*15*), although we were unable to identify the minor photoproduct under these conditions. In D_2O, however, the relative yield of 17α-TBOH photoproducts was reversed from that observed in H_2O, thereby allowing identification of the unknown photoproduct. Specifically, photolysis in D_2O yielded a 6:1 mixture of a major product and residual 17α-TBOH (Fig. S1), as well as various trace components (one of which was 12-hydroxy-17α-TBOH). 2D NMR experiments on this sample revealed that the C- and D-rings and the olefin unit in the B-ring remained intact in the major product, indicating that the difference between this product and 17α-TBOH must be primarily associated with the A-ring. The impurity of the sample precluded complete assignment of all NMR signals, and the scale and mixture complexity precluded isolation of sufficient quantity of material for further analysis. However, when NMR data were combined with MS data indicating product molecular formula and UV/vis spectrum data from LC-DAD (Fig. S2) for the major component indicating replacement of the trienone system (λ_{max} 350) with a diene chromophore (λ_{max} 245), this product was assigned the 5-hydroxy-17α-TBOH analog structure.

NMR Support for Product-to-Parent Reversion.

Analysis of the 17β-TBOH photoproduct mixture after storage in the dark for 6 days (Fig. S3) indicated the presence of 17β-TBOH (arising from reversion, reference NMR spectrum provided in Fig. S4) and a previously identified and fully characterized (*15*) dialdehyde decomposition product (reference NMR spectrum shown in Fig. S5) in a 5:1 ratio, as well as multiple trace components. Diagnostic features of the dialdehyde decomposition product include the proton signals at δ_H 9.13 and δ_H 9.99. After 6 days in the dark, the 17α-TBOH photoproduct mixture (Fig. S6) primarily contained 17α-TBOH (reference NMR spectrum shown in Fig. S7), but analysis also indicated the presence of a minor, analogous dialdehyde decomposition product (diagnostic features: δ_H 9.47 and δ_H 10.01). The 17β-TBOH photoproduct mixture analyzed immediately after adjustment to pH 2 (Fig. S8) indicated the presence of 17β-TBOH, with minimal trace components.

In a complementary effort to monitor a complete reversion cycle (i.e. photolysis and dehydration) via NMR, a sample of 17α-TBOH was subjected to photodegradation in D_2O (pH 7), concentrated, and re-dissolved in CD_3OD for NMR analysis (Fig. S9; data for TBA metabolite and photoproduct standards had been collected using CD_3OD to enhance solubility). The sample consisted of a deuteriated analog of 5-hydroxy-17α-TBOH, with other trace components present. HRESITOFMS analysis of a subsample collected at this point supported the presence of a compound with the formula $C_{18}H_{22}D_2O_3$ (*m/z* 313.1755 $[M+Na]^+$ calcd. for $C_{18}H_{22}D_2O_3Na$, 313.1749), confirming the addition of D_2O in the photodegradation process, and supporting the proposed structure of the analog. The sample was redissolved in D_2O, stored in the dark, and monitored by NMR every few days. After 13 days (Fig. S10), the amount of a 17α-TBOH-like compound exceeded the amount of 5-hydroxy-17α-TBOH analog present. HRESITOFMS analysis indicated the presence of a new major ion with the molecular formula of $C_{18}H_{21}DO_2$ (*m/z* 294.1609 $[M+Na]^+$ calcd. for $C_{18}H_{21}DO_2Na$, 294.1580). This result, coupled with key observable ^1H NMR signals (absence of the singlet at δ_H 5.68, but otherwise matching those of 17α-TBOH) led us to conclude that a deuteriated version of 17α-TBOH was regenerated with a deuterium atom in the 4-position, as would be expected for regeneration from the deuterium-containing 5-hydroxy-17α-TBOH analog.

17β-TBOH and TBO Diurnal Cycling.

Results from day-night cycling experiments for 17β-TBOH and TBO, analogous to data shown in Figure 1A of the main text for 17α-TBOH, are shown in Fig. S11. For both 17β-TBOH and TBO, two major photolysis products were observed. In each case, we have previously (*15*) identified one of these products (indicated in the Figure) as the C12 hydroxylated analog of each metabolite (i.e., "12-hydroxy-17β-TBOH" and "12-hydroxy-TBO"). By analogy to the above NMR results for 17α-TBOH, we propose that the second photoproduct in each case is the corresponding 5-hydroxy analog of 17β-TBOH and TBO.

Relative to 17α-TBOH, a key difference observed for 17β-TBOH and TBO is the decay of their photoproducts during irradiation. Such instability during irradiation was not observed for 17α-TBOH photoproducts, and the rate of 17β-TBOH and TBO photoproduct decay in the presence of light was roughly 2-fold greater than observed in the dark. The relative rate of photoproduct decay in the absence of light is also notable. For example, assuming exponential decay, the pseudo-first-order rate constants (k_{obs} values) for the decay of the 12-hydroxy analogs of 17α-TBOH and 17β-TBOH are 0.017 (±0.001) and 0.019 (±0.005) h^{-1}, respectively (values represent the mean and standard deviation of the three rate constants measured during each dark

period). Despite these statistically indistinguishable rate constants for dark (thermochemical) transformation, a larger fraction of 12-hydroxy-17α-TBOH decay is attributable to dehydration that regenerates 17α-TBOH. The lesser extent of dehydration occurring for 12-hydroxy-17β-TBOH is presumably due to a faster rate of reaction with water and/or hydroxide ions to yield higher order hydroxylated products or the 11,12-dialdehyde decomposition product we have previously identified in 17β-TBOH systems (*15*).

pH-dependent Trends in the Photolysis Rate of 17α-TBOH**.**

The pH-dependent rate of 17α-TBOH photolysis (compared at pH 5 and 7) is shown in Fig. S12. At pH 5, the half-life for photolysis was roughly 6-fold longer than that observed initially at pH 7, although the rate of phototransformation at pH 7 did slow over time. These trends reflect the contribution of photoproduct dehydration as a source for 17α-TBOH in our closed experimental systems. At pH 5, the faster (i.e., acid-catalyzed) rate of photoproduct dehydration (see Figure 2B) ultimately slows the net rate of 17α-TBOH decay during irradiation. Similarly, the non-linearity in the plot of ln[17α-TBOH] versus time at pH 7 is explained by these concurrent reactions. As 5- and 12-hydroxy-17α-TBOH accumulate over time in our experimental systems, so too do their rates of dehydration. Accordingly, the slower kinetic regime observed over long timescales at pH 7 must reflect the point along the reaction coordinate where the cumulative rate of photoproduct dehydration is on the order of that for photolysis. At pH 7, this point of nearly equivalent rates of photolysis and dehydration appears to occur after ~95% transformation of 17α-TBOH.

Formation of TBO Analogs during Acid-Catalyzed Photoproduct Dehydration.

LC-DAD and LC-HRMS/MS analysis suggest that photoproduct dehydration at pH 5 produces structural analogs of TBO. Fig. S13 compares LC-DAD traces collected during the analysis of TBO photoproduct mixtures that were stored in the dark for up to 144 h at pH 5 and pH 7. Over time at both pH values, evidence of TBO formation via reversion was observed. However, at pH 5, regrowth of TBO was accompanied by the occurrence of a second peak in our LC-DAD trace eluting immediately before that of TBO. Notably, this peak was not observed at pH 7. Analysis of TBO photoproduct mixtures using LC-HRMS/MS (as described in our earlier work (*15*)) indicated that the corresponding product mass spectra were essentially indistinguishable from TBO, suggesting strong structural similarities between this product and TBO (Figs. S14-16).

Analogous to our proposed mechanism for acid-catalyzed dehydration of 5- and 12-hydroxy-17α-TBOH (Figure 3), protonation and loss of H_2O from TBO photoproducts generates a carbocation. Previous work exploring dehydration of a C17-hydroxylated 4,6-dien-3-one in concentrated sulfuric acid observed such carbocation intermediates to be prone to methyl and hydride migrations, in addition to π-bond shifts, during formation of the corresponding 4,6,8-trienone (*28*). In fact, our theoretical calculations suggest that such structural arrangements can result in thermodynamically preferred end products (i.e., an analog or isomer that exhibits a lower free energy than TBO). For example, Fig. S17 illustrates a proposed formation pathway that could lead to a more thermodynamically favorable isomer (Structure III), which is ~8 kcal/mol lower in free energy than TBO. Notably, this isomer is also more thermodynamically favorable than possible isomers generated via deprotonation at either C6 (Structure I) or C8 (Structure II).

While the above analysis is not definitive and requires further investigation, our experimental evidence clearly points to more complex reaction pathways for TBO photoproduct reversion at pH 5 than at pH 7. For example, trends in data collected at pH 5 are consistent with photoproduct interconversion, presumably mediated via the carbocation intermediate responsible for analog formation (Fig. S18). Specifically, the peak associated with the minor photoproduct (12-hydroxy-TBO) quickly decays, while the response attributable to the major photoproduct (presumed 5-hydroxy-TBO) increases over this same time interval. Such behavior was not observed for TBO at pH 7or for any other TBA metabolite in our studies.

Field Photolysis Studies of Photoproduct-to-Parent Reversion.

As discussed in the main text (Figure 4), 17α-TBOH derived by leaching TBA-implanted cattle manure exhibits concentration trends consistent with our expectations for product-to-parent reversion under realistic conditions representative of those frequently encountered in agricultural receiving waters (i.e., manure from TBA-implanted cattle contacted with a natural sunlit surface water). While performing this 17α-TBOH analysis using GC-MS/MS with MSTFA-I_2 derivatization to enhance chromatography (*26, 27*), we noted the occurrence of a prominent non-target peak in MS/MS transitions used for quantification of 17α-TBOH that also exhibited similar reversion dynamics consistent with those observed for 17α-TBOH (Fig. S20). Upon further analysis, the full scan mass spectra of this non-target peak exhibited substantial similarities to spectra for known TBA metabolites, particularly the twin high mass spectra pairs and *m/z* 368 fragment ion similar to that observed for TBO (Fig. S21).

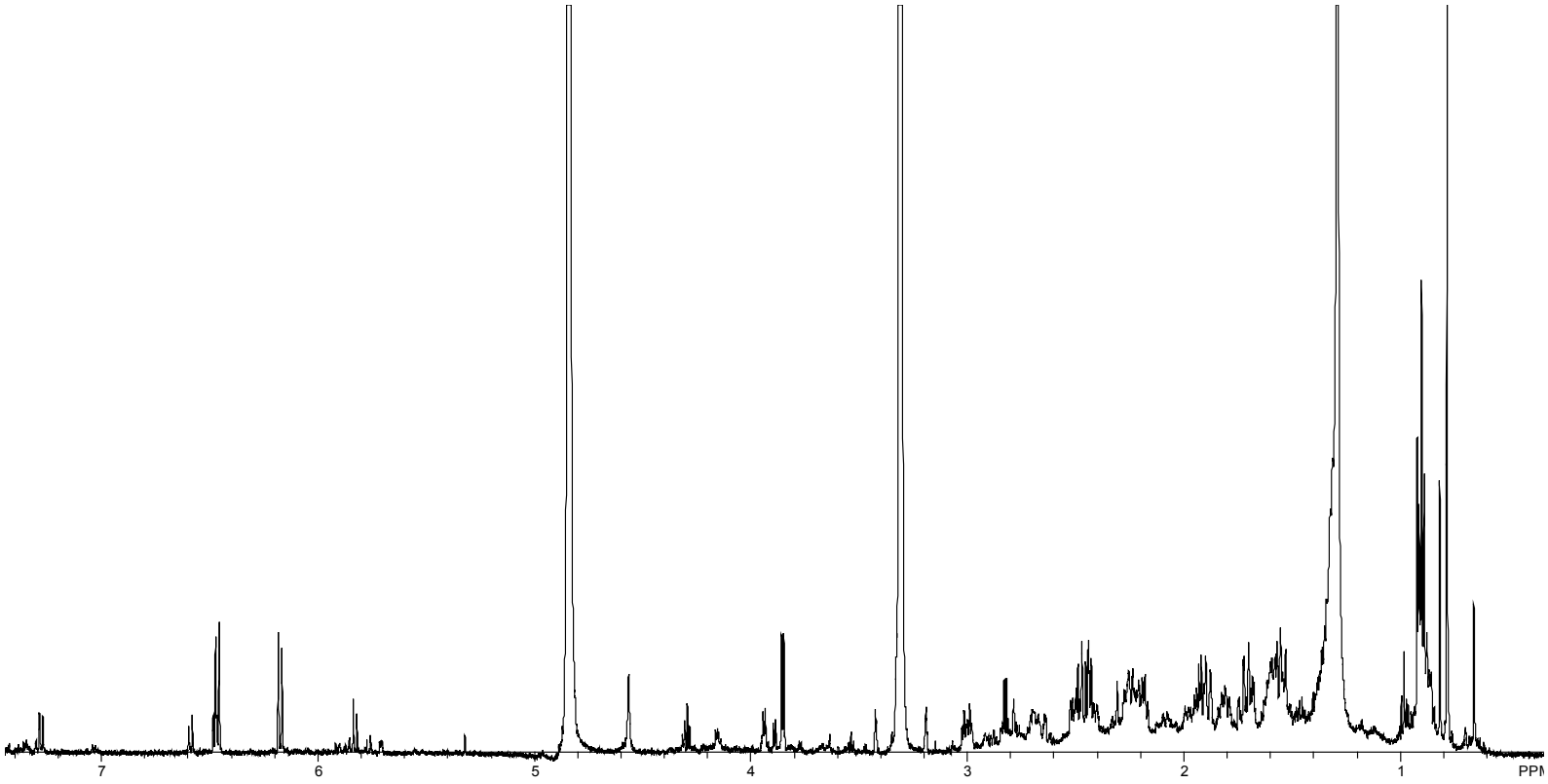

Fig. S1.

^{1}H NMR spectrum (500 MHz; CD_3OD) of product mixture arising from photodegradation of 17α-TBOH in D_2O containing (deuteriated) 5-hydroxy-17α-TBOH as the major product.

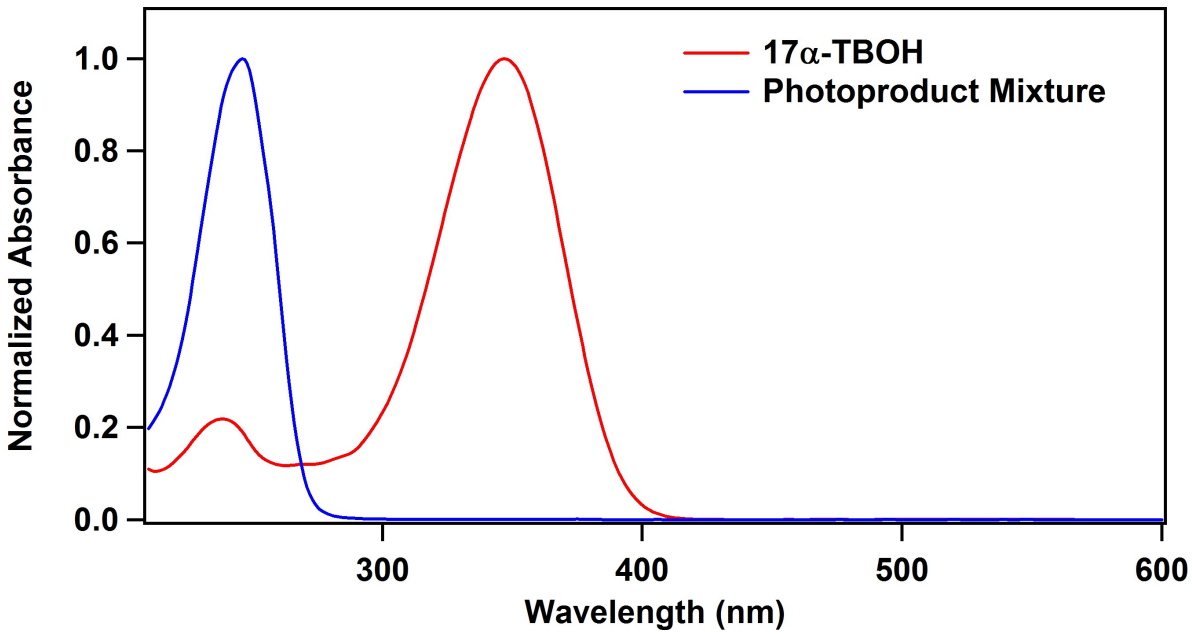

Fig, S2.

UV-visible spectrum comparison of 17α-TBOH and its major photodegradation product observed in D_2O at pH 7 (assigned as 5-hydroxy-17α-TBOH). Spectra are normalized to emphasize difference in wavelength.

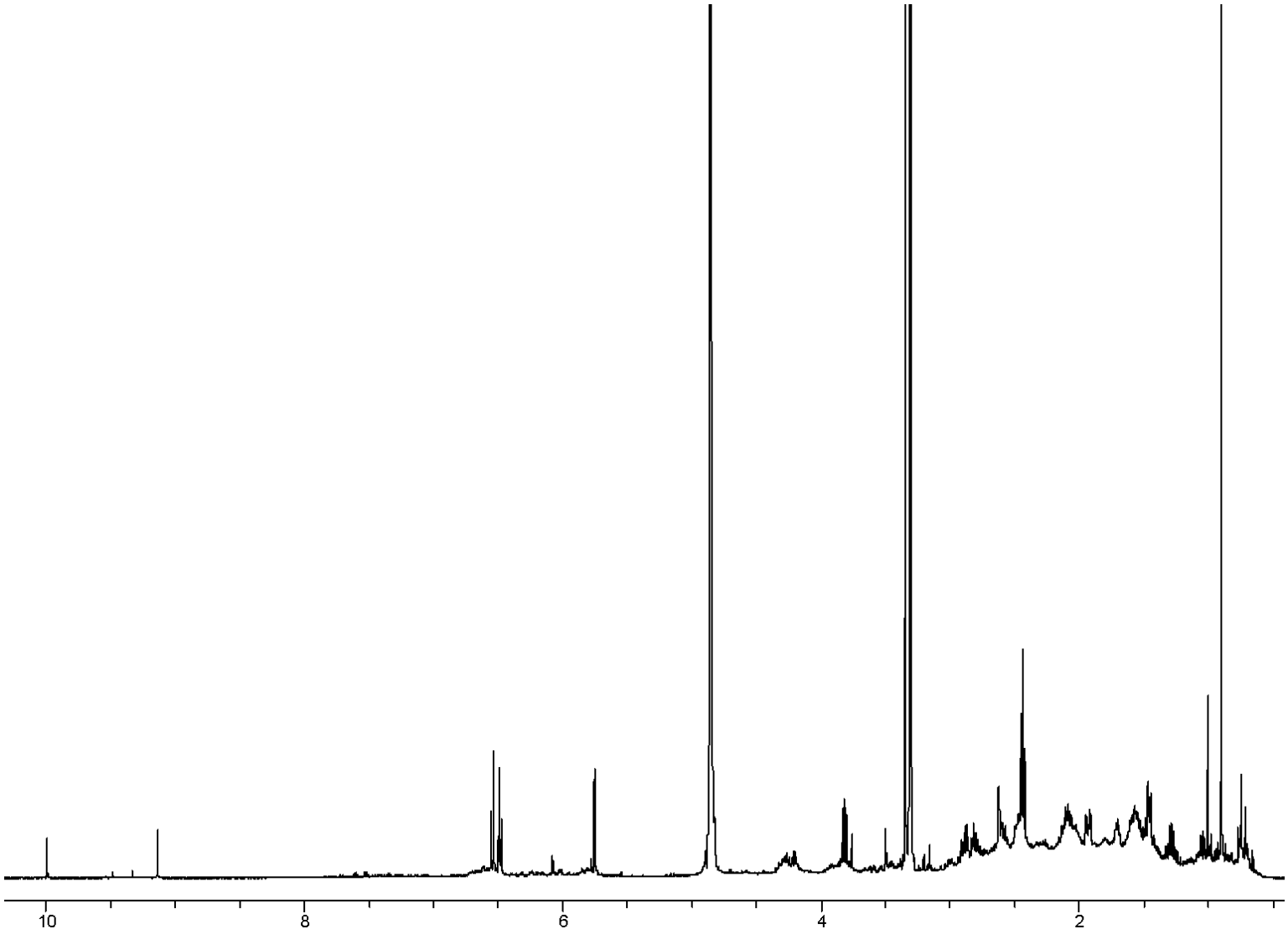

Fig. S3.

^{1}H NMR spectrum (500 MHz) of 17β-TBOH day 6 product mixture in CD_3OD.

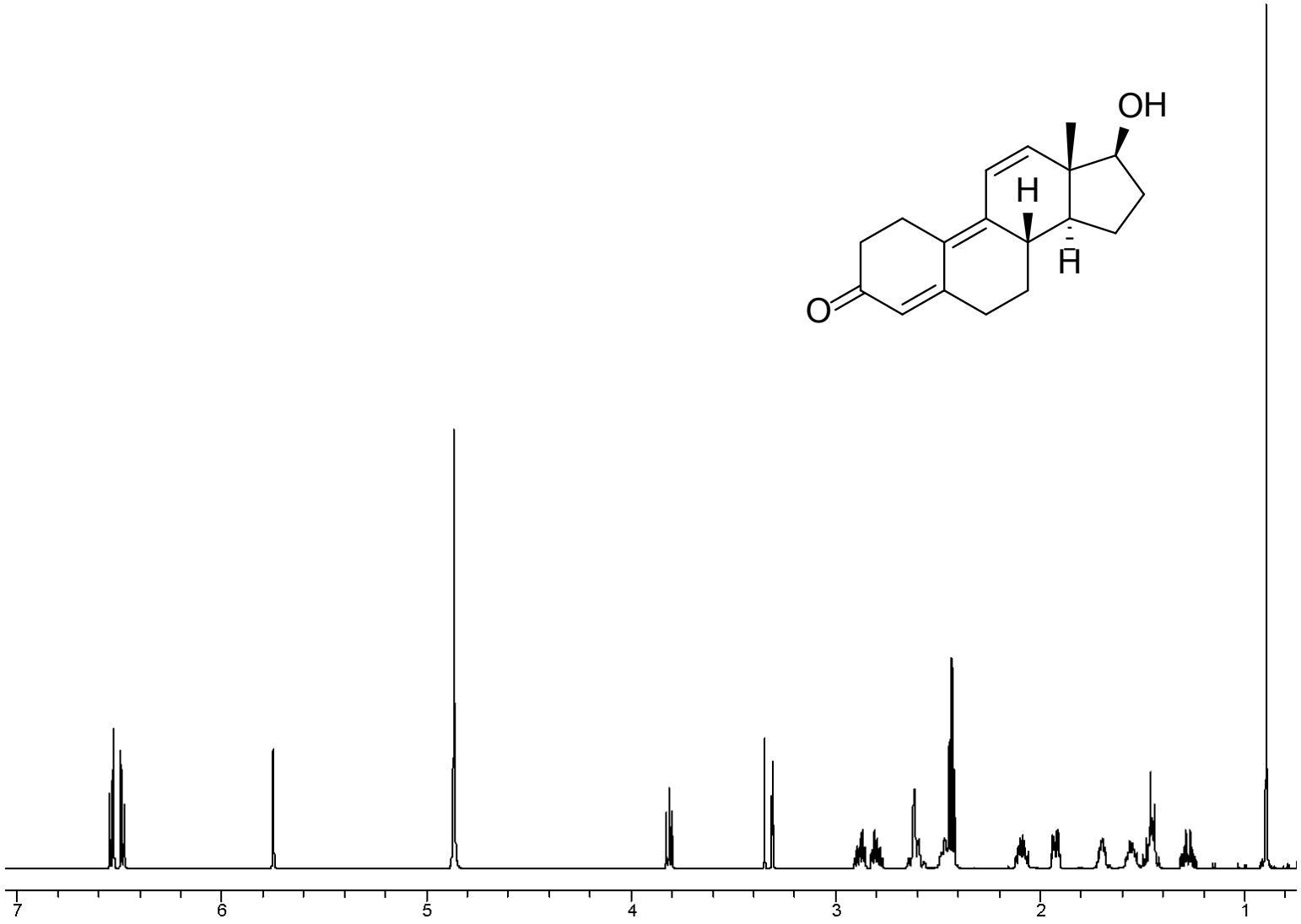

Fig. S4.
^{1}H NMR spectrum (500 MHz) of 17β-TBOH in CD_3OD.

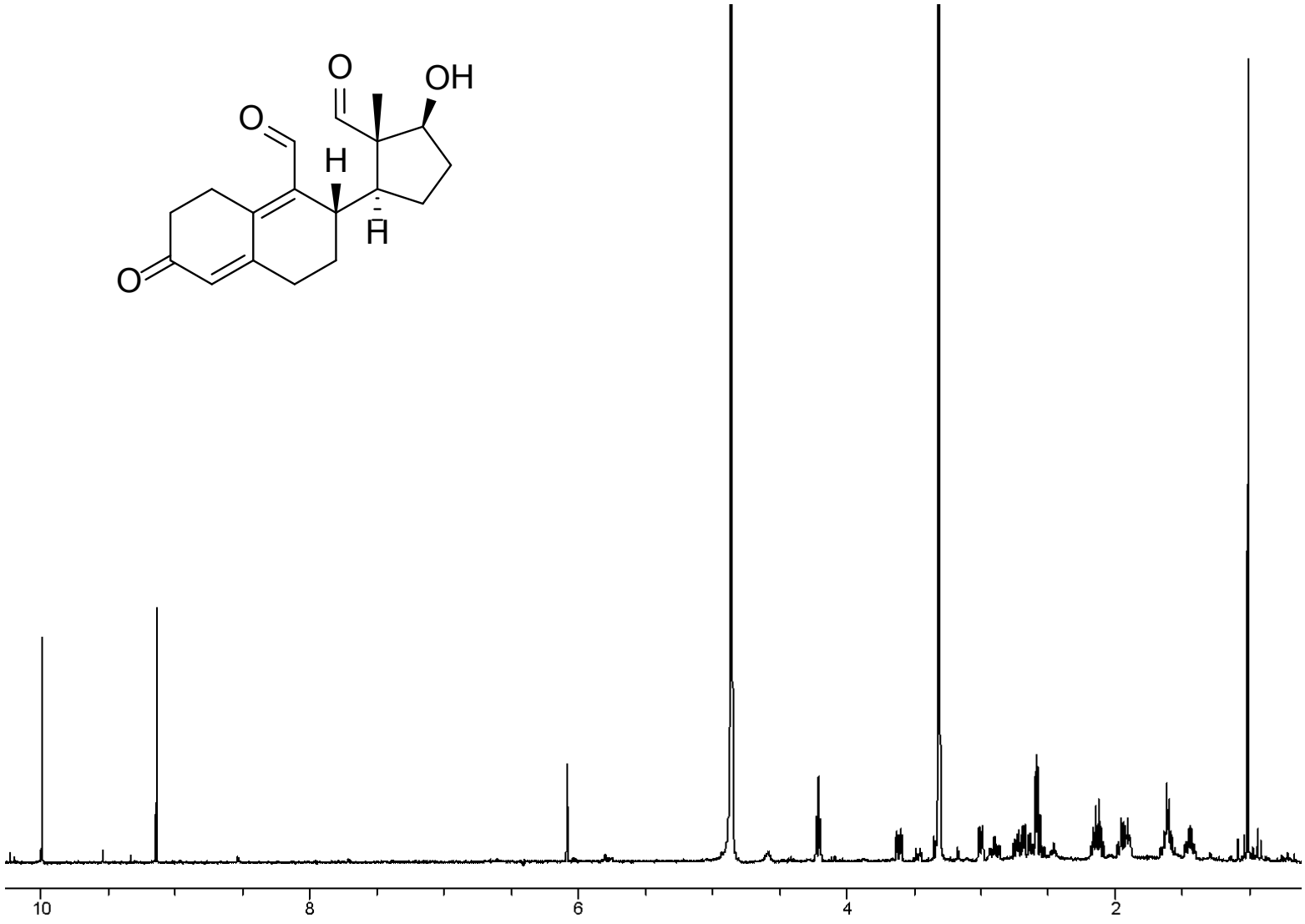

Figure S5.

^{1}H NMR spectrum (500 MHz) of dialdehyde decomposition product in CD_3OD.

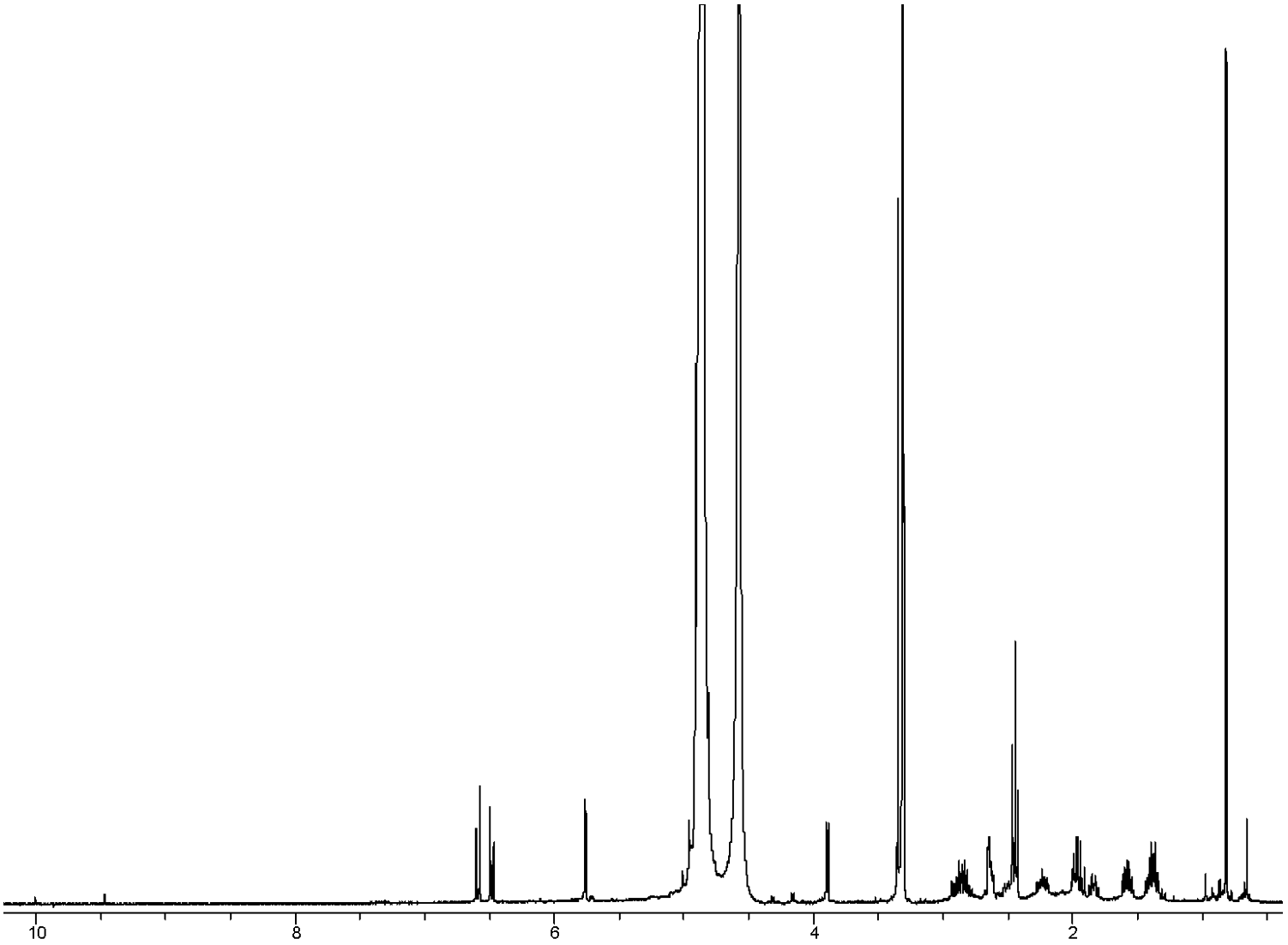

Figure S6.

^{1}H NMR spectrum (500 MHz) of 17α-TBOH day 6 product mixture in CD_3OD.

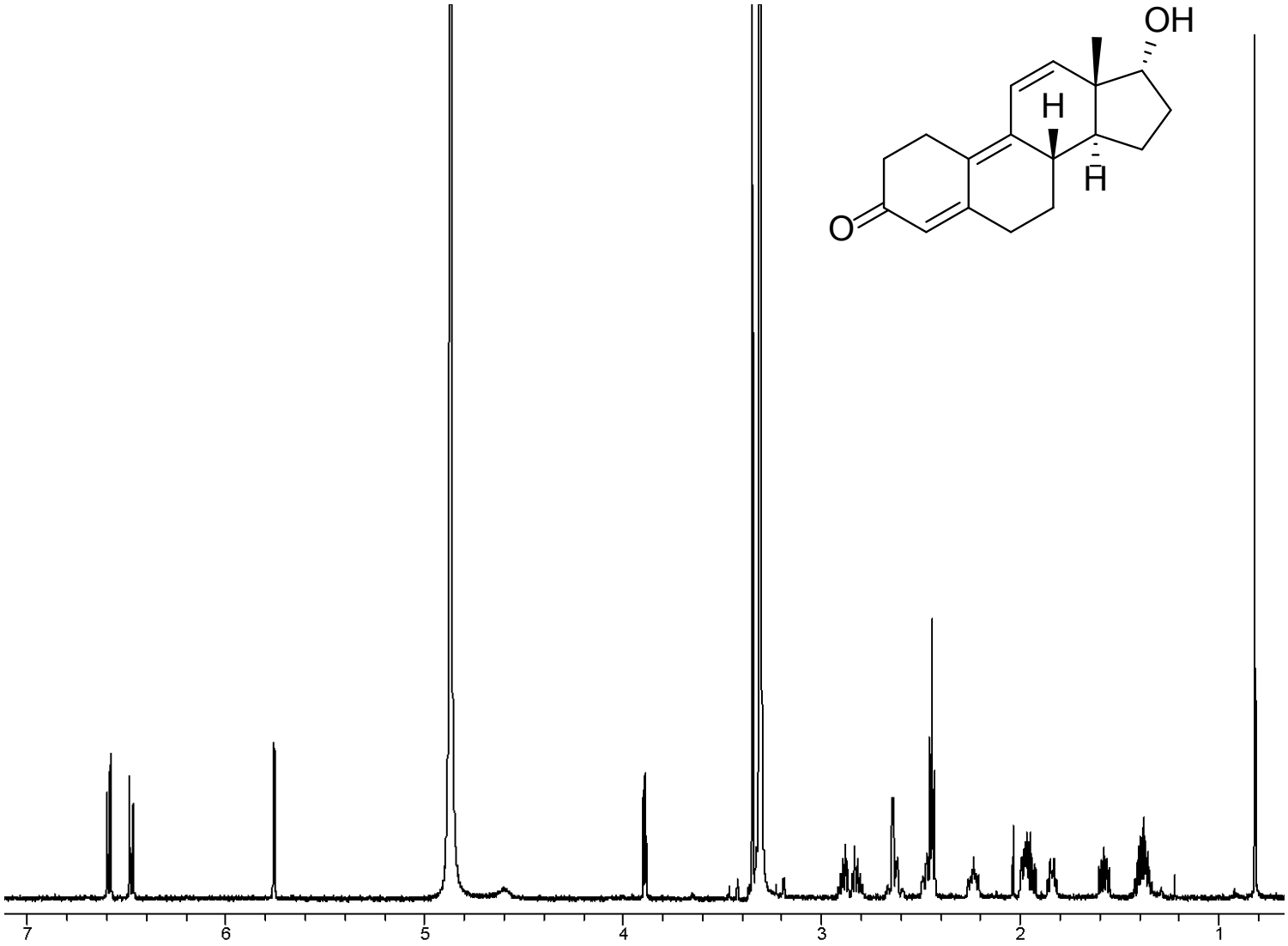

Figure S7.

^{1}H NMR spectrum (500 MHz) of 17α-TBOH in CD_3OD.

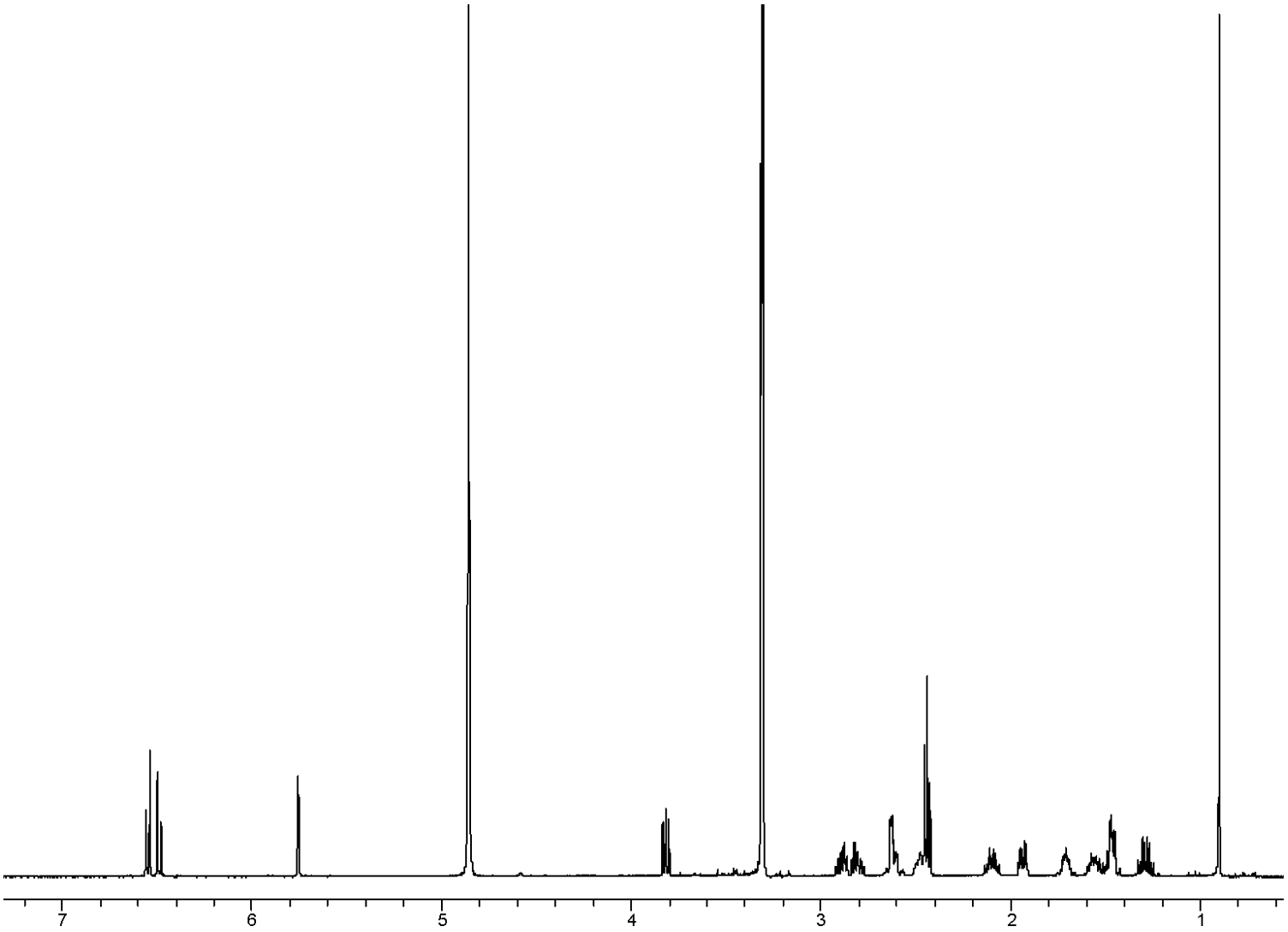

Figure S8.
^{1}H NMR spectrum (500 MHz) of 17β-TBOH products at pH 2 (in CD_3OD).

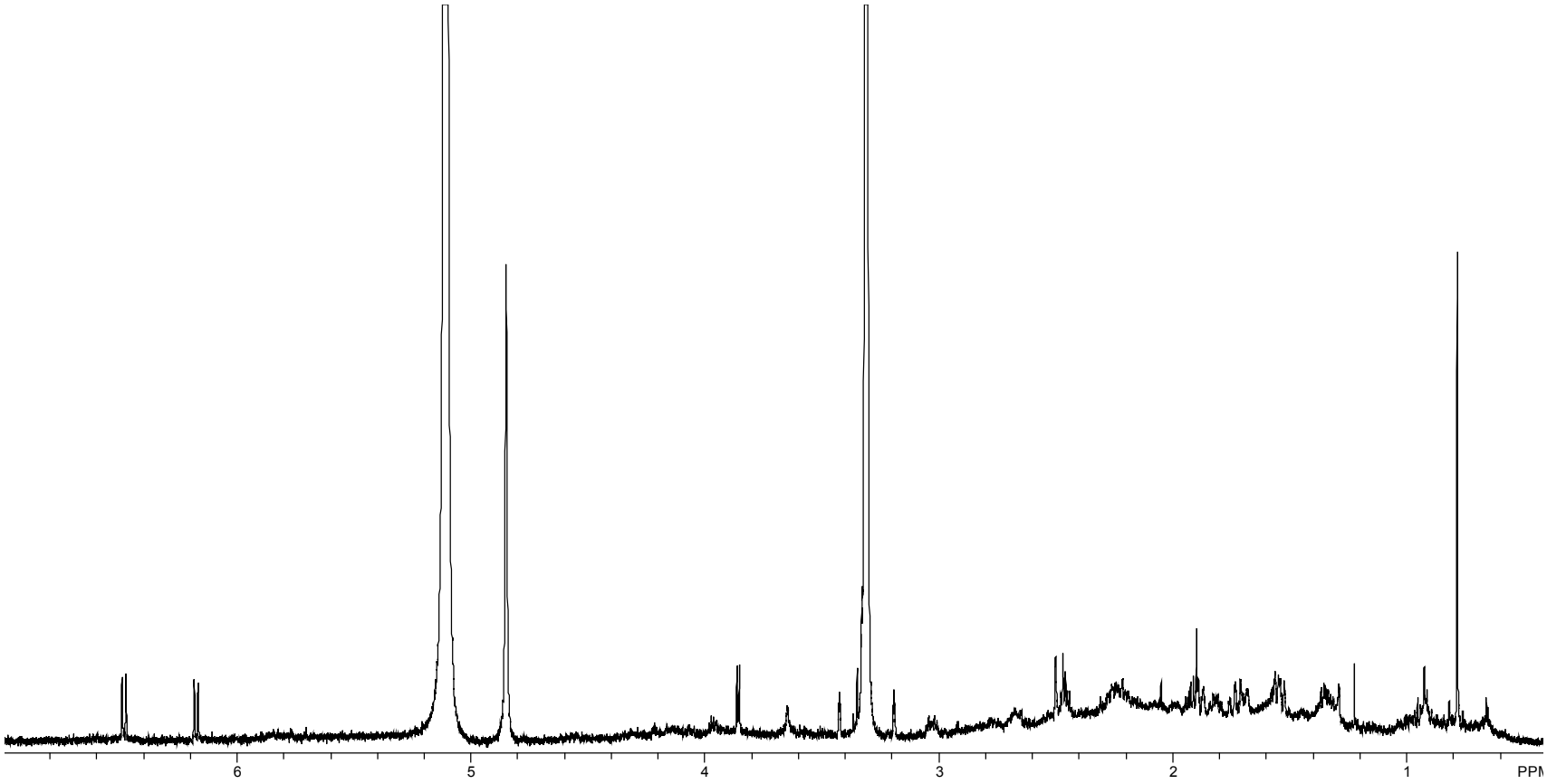

Fig. S9.

^{1}H NMR spectrum in CD_3OD (500 MHz) of initial product mixture arising from photodegradation of 17α-TBOH in D_2O, containing (deuteriated) 5-hydroxy-17α-TBOH as the only major product.

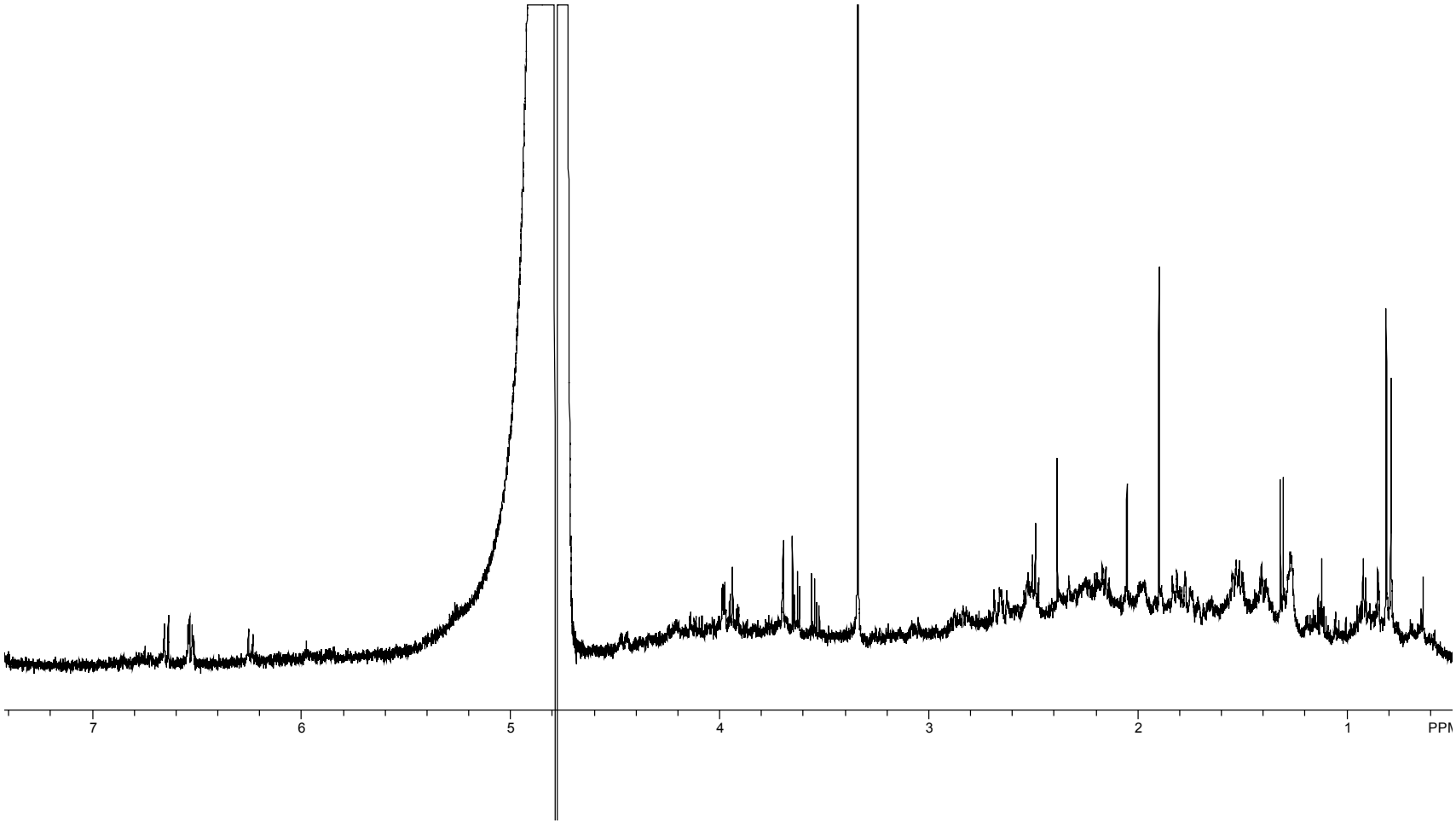

Fig. S10.

^{1}H NMR spectrum in D_2O (500 MHz) of product mixture arising from photodegradation of 17α-TBOH in D_2O after 13 days showing partial regeneration of (deuteriated) 17α-TBOH along with 5-hydroxy-17α-TBOH analog.

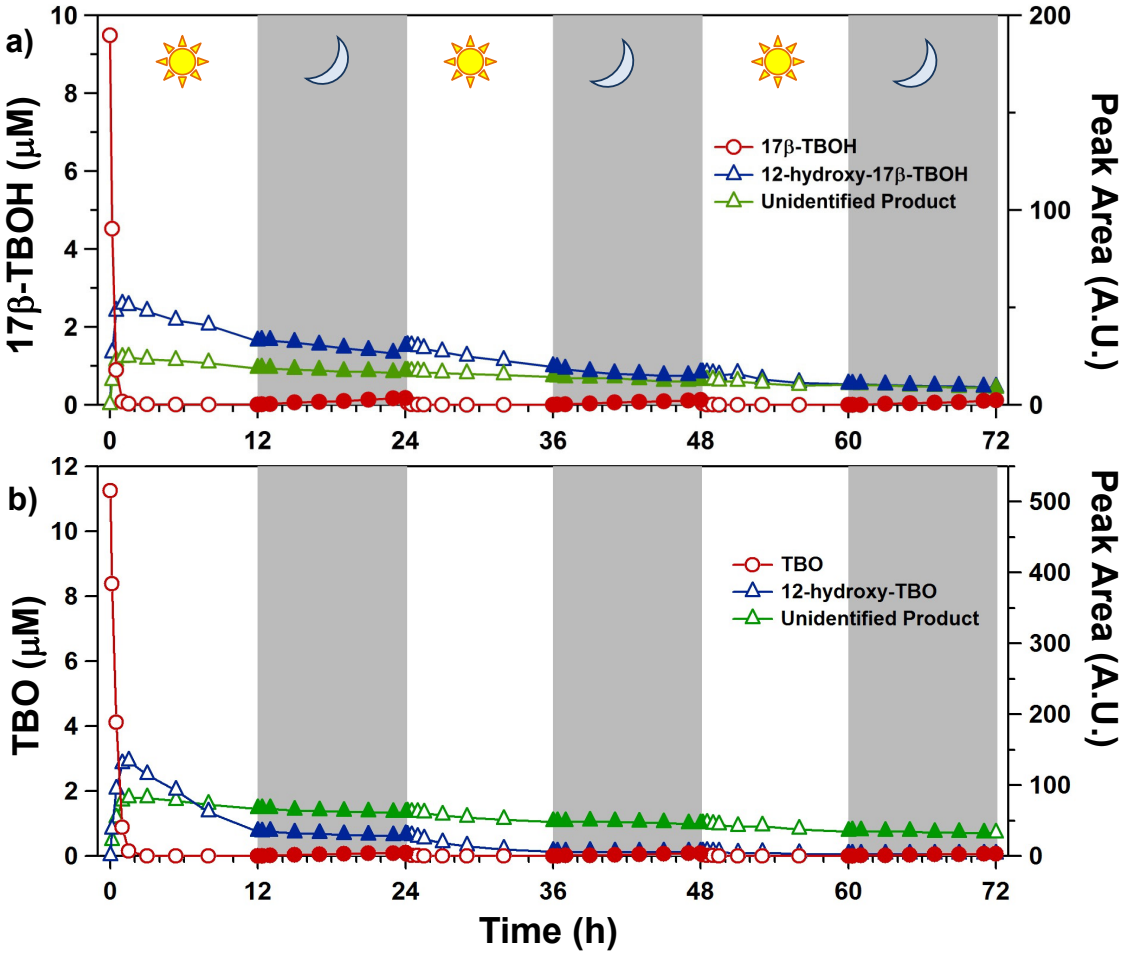

Fig. S11.

Day-night cycling of (a) 17β-TBOH and (b) TBO at pH 7 and 25°C. Also shown are trends in the formation of the two major photoproducts observable via diode array detection for 17β-TBOH and TBO. One of these products is the 12-hydroxy analog of each metabolite, while the unidentified photoproduct is most likely the corresponding 5-hydroxy analog that we have confirmed via NMR and LC/MS/MS analysis as a photoproduct of 17α-TBOH phototransformation. Data for 17β-TBOH and TBO are presented as aqueous concentration (left axis), whereas peak area measurements corresponding to spectrophotometric absorbance (at λ = 350 nm for 17α-TBOH and λ = 254 nm for 5- and 12-hydroxy analogs) are also presented (right axis). Data collected during simulated solar irradiance are shown as open symbols whereas data collected in the absence of light (shaded grey areas) are shown as solid symbols.

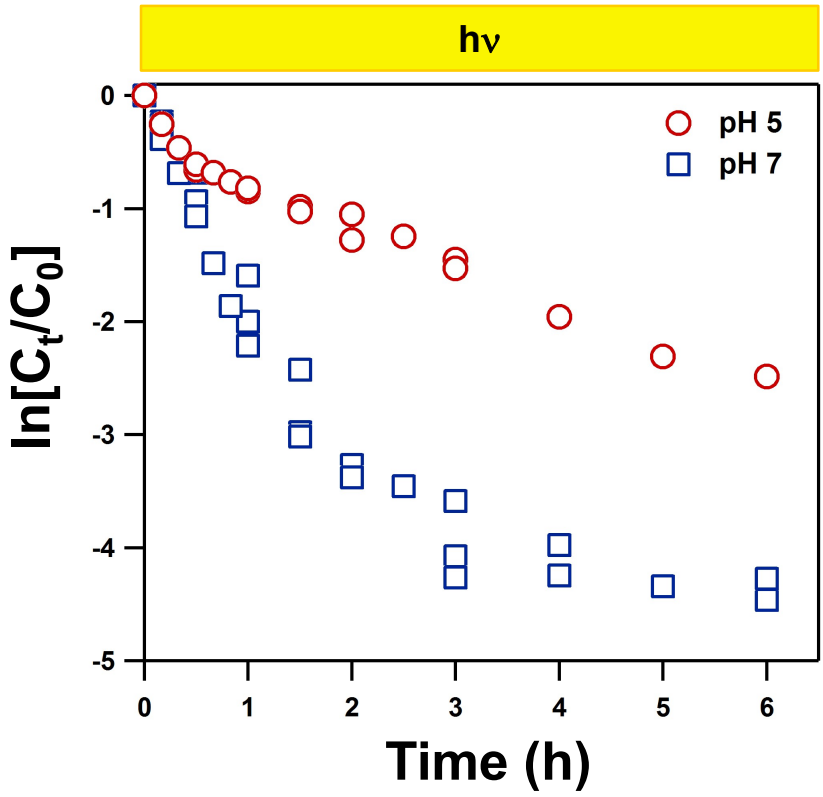

Fig, S12.

Semi-log plot of 17α-TBOH concentration as a function of irradiation time (with simulated sunlight) at pH 5 (red) and pH 7 (blue). The greater, acid-catalyzed rate of dehydration at pH 5 results in a slower net rate of direct photolysis, producing a greater effective half-life for 17α-TBOH in slightly acidic water. While the rate of photolysis slows both at pH 5 and over longer timescales at pH 7, loss in 17α-TBOH concentration was observed throughout the duration of these experiments. Thus, a photostationary state (i.e., photochemical "equilibrium") was not achieved in these systems. Notably, slower rates of 17α-TBOH phototransformation at pH 5 relative to pH 7 were observed in TBA manufacturer regulatory studies, but attributed, we believe incorrectly, to cloudy conditions (*12*).

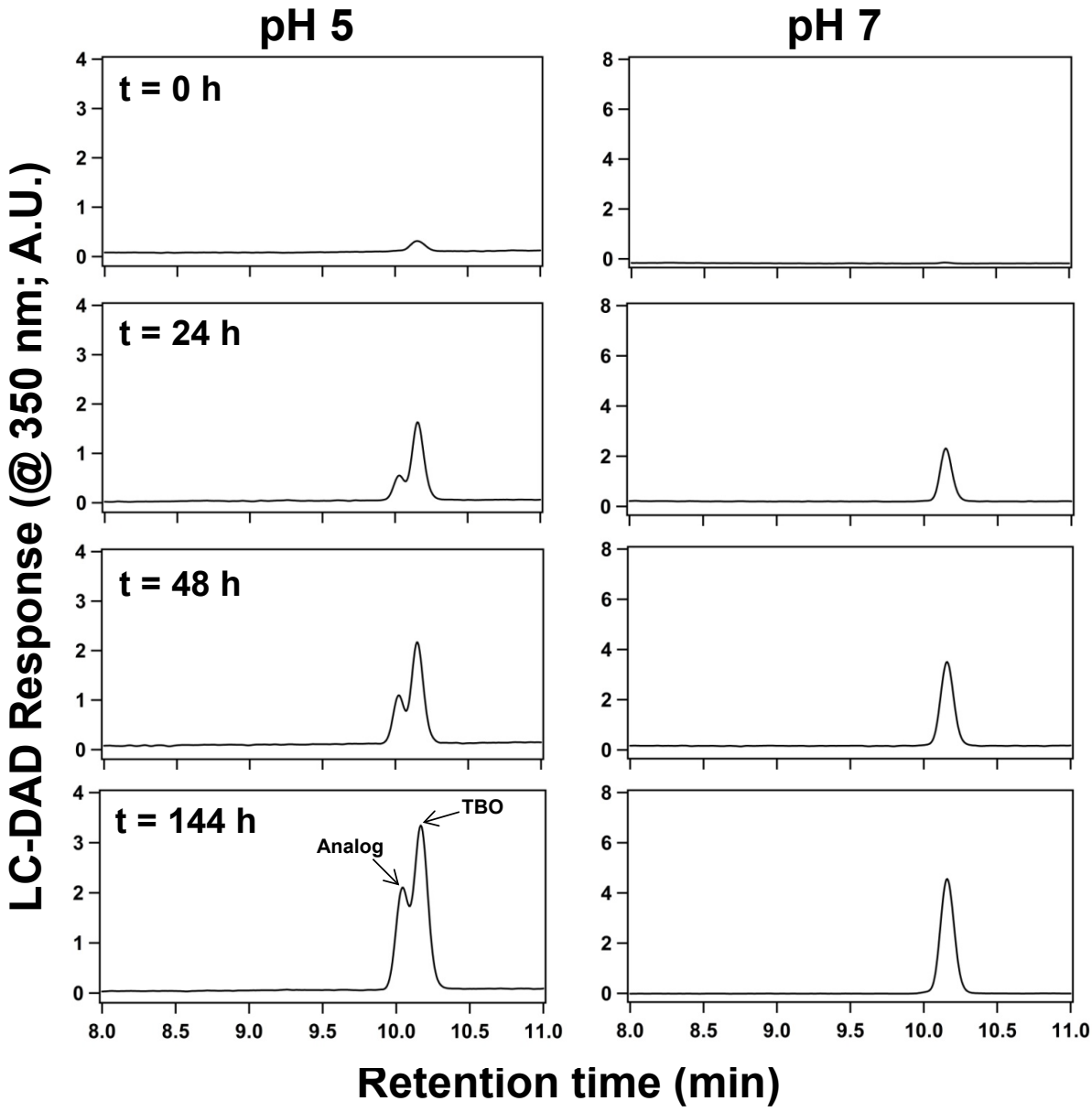

Fig. S13.

LC-DAD traces obtained from analysis of TBO product mixtures stored in the dark at either pH 5 (left) or pH 7 (right). At pH 7, product-to-parent reversion results in the regrowth of TBO over time (up to 144 h), as indicated by the increasing DAD response (at λ = 350 nm) for the peak characteristic of TBO (at ~10.2 minutes elution time). In contrast at pH 5, reversion is accompanied by the formation of an as yet unidentified TBO analog, as evidenced by the split or co-eluting peak observed in the LC-DAD trace when using our standard analytical method. Altering chromatographic conditions (i.e. solvent composition) is capable of achieving baseline separation between these peaks (data not shown).

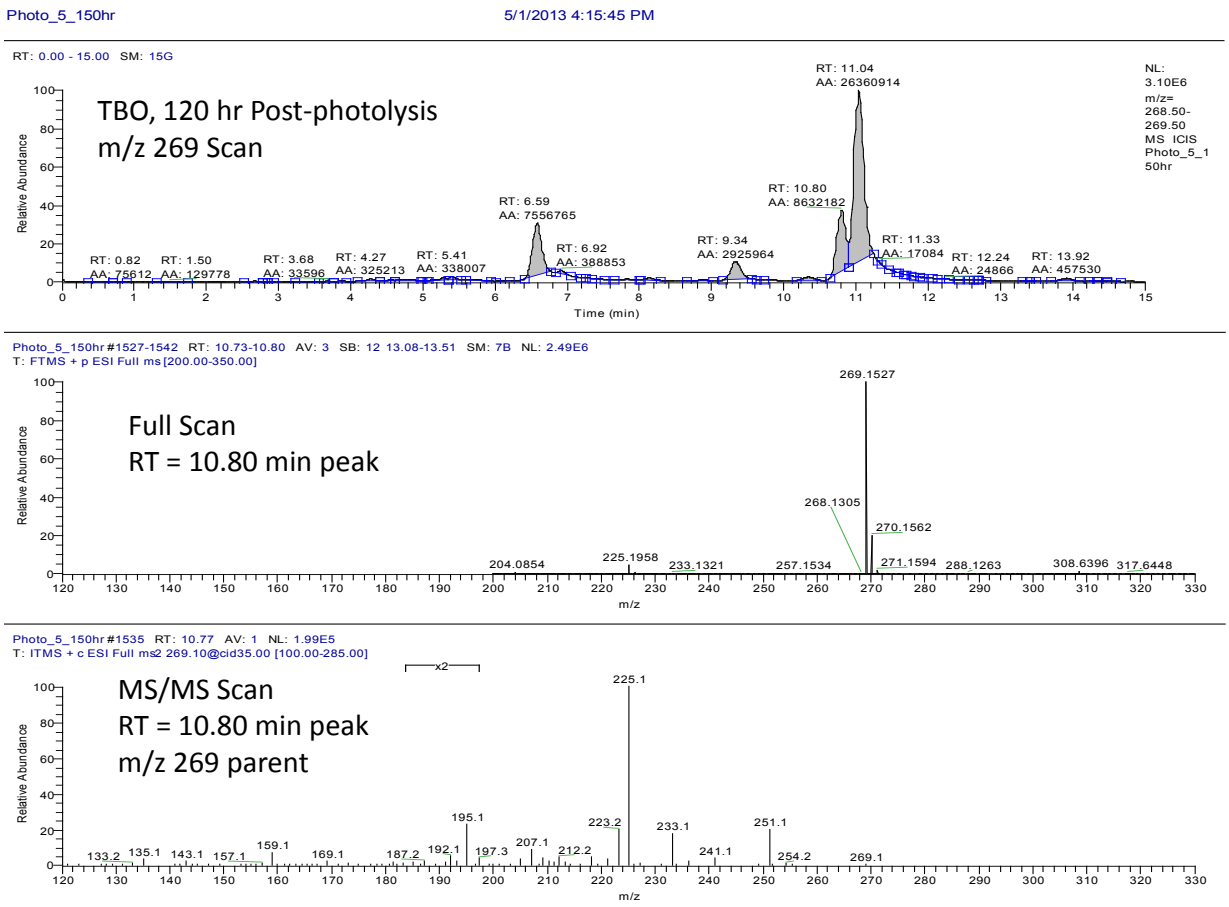

Fig, S14.

LC-HRMS/MS chromatogram and spectra demonstrating TBO (11.04 minute peak), formed via product-to-parent reversion at 120 hr post-photolysis, and also the TBO structural analog at 10.80 minutes. The residual peak at 6.39 minutes represents the photoproduct 12-hydroxy-TBO, which reverts back to TBO and the 10.80 minute structural analog. Full scan and MS/MS data for both TBO and the structural analog are essentially identical, suggesting that they cannot be distinguished from each other by mass spectrometry.

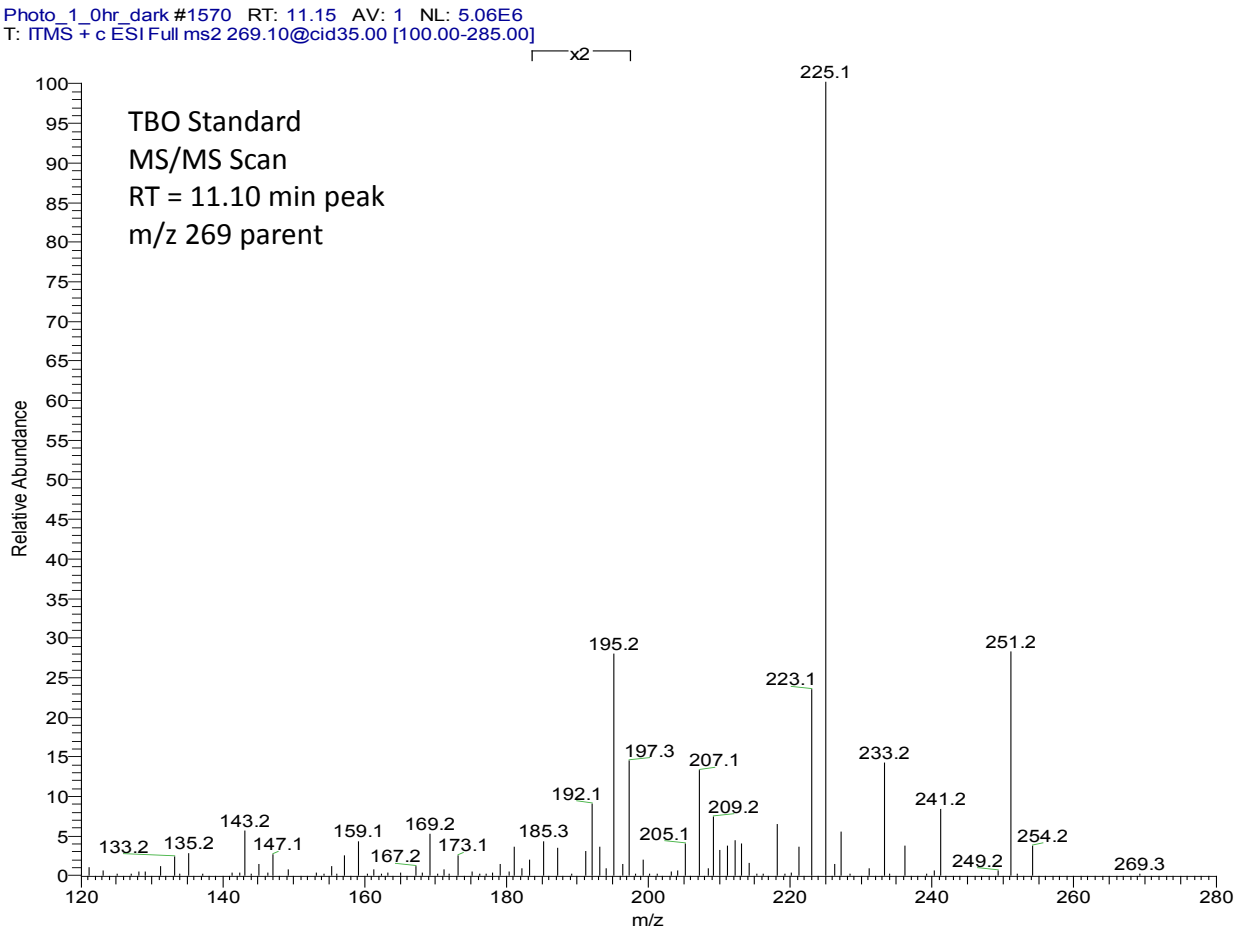

Fig. S15.

MS/MS data for the parent ion of a TBO standard (retention time 11.15 minutes) collected from the initial 0 hr sample at pH 5.

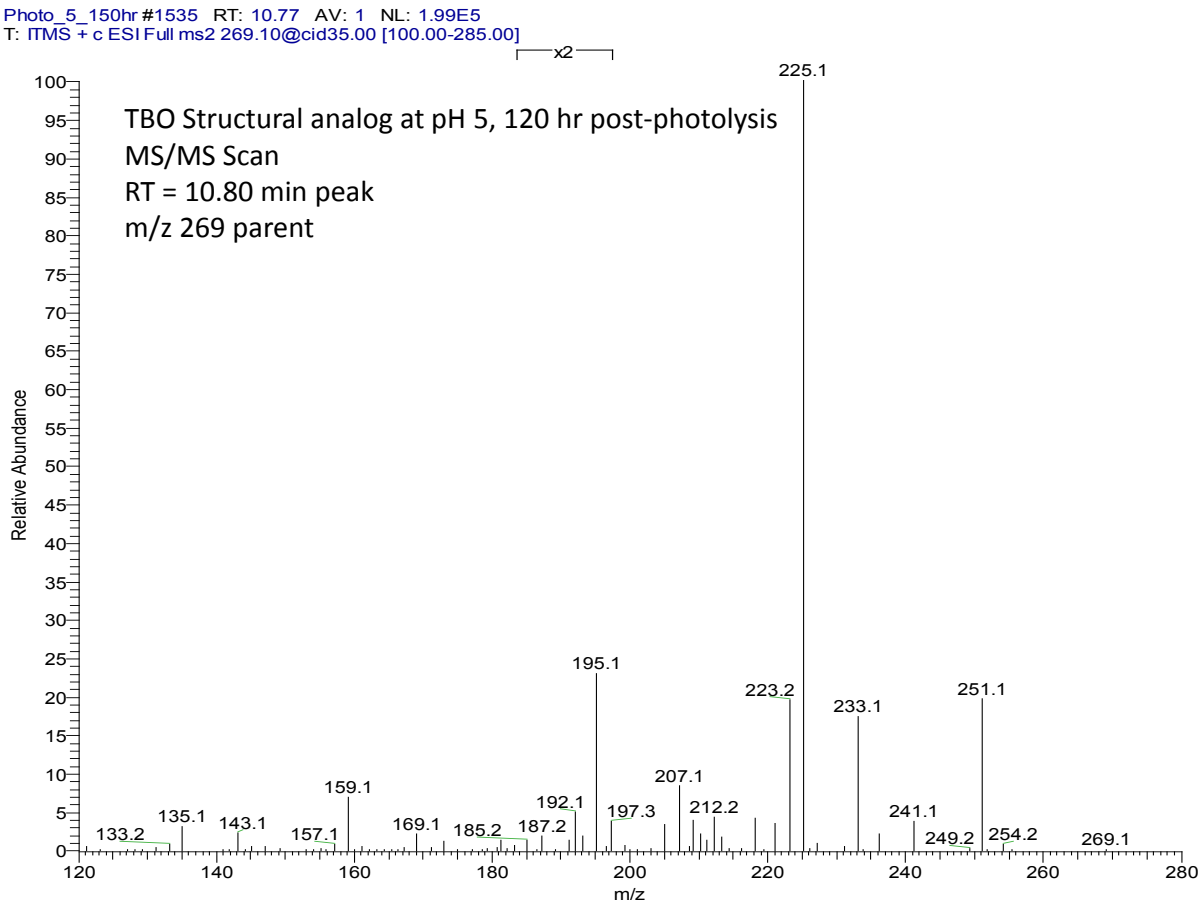

Fig. S16.
MS/MS data for the TBO structural analog (retention time 10.77 minutes) at 120 hr post-photolysis at pH 5.

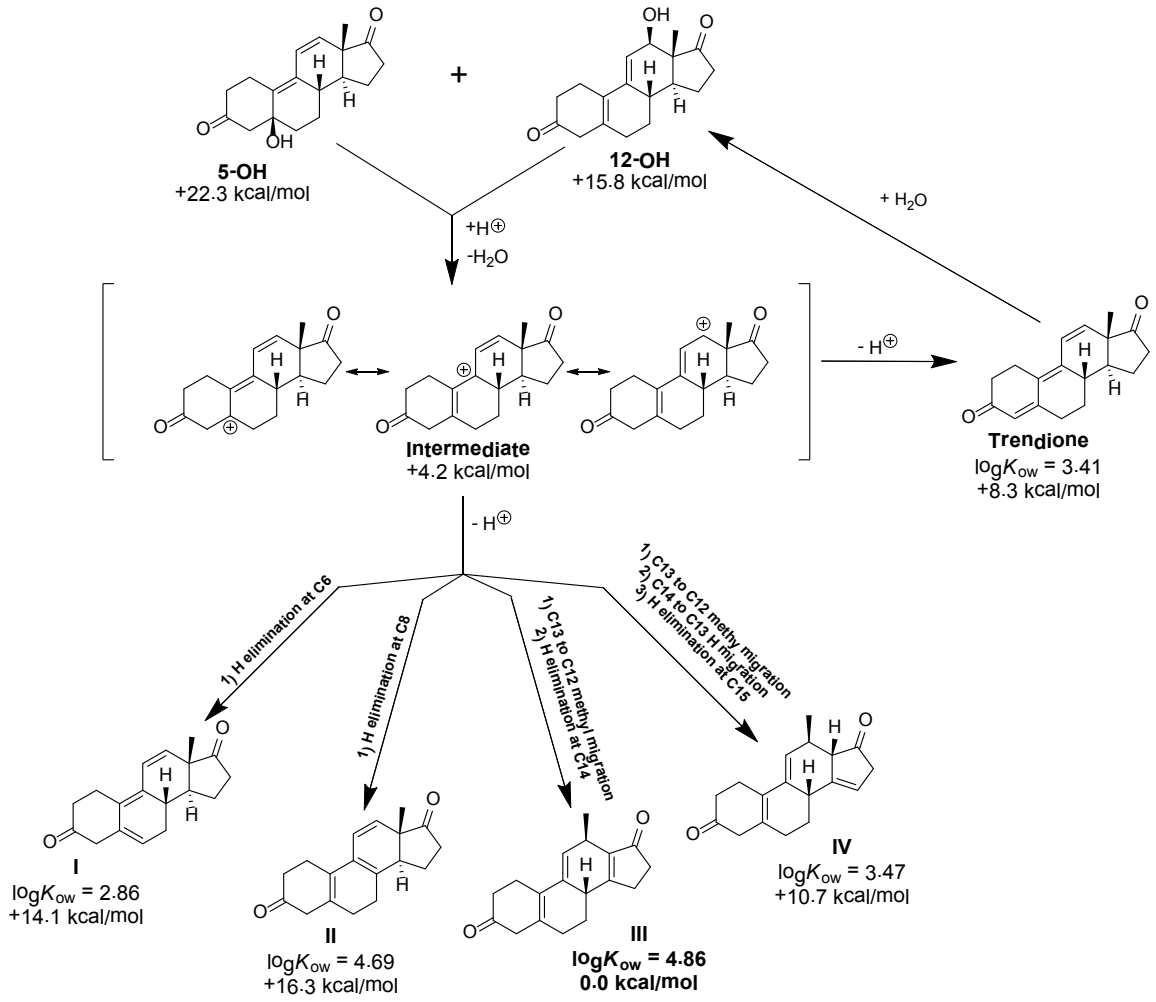

Figure S17.

Relative Gibbs free energies for possible TBO isomers under acidic pH conditions. All free energies are reported relative to Structure III, the most thermodynamically favorable species, with its values indicated in bold. Also noted is the formation pathway for each analog derived from the proposed resonance-stabilized carbocation intermediate formed during acid-catalyzed dehydration of hydroxylated TBO photoproducts. Because the analog observed in Figure S13 was observed to co-elute with TBO during LC-DAD analysis, we have also provided estimates of octanol-water partitioning coefficients (log K_{ow} values) for each proposed TBO analog. While Structure III possesses a logK_{ow} value almost 1.5 units greater than TBO, structure IV (which possesses a Gibbs free energy comparable to TBO (+2.4 kcal/mol)) has an essentially equivalent estimated logK_{ow} value. This analog would therefore be expected to exhibit similar chromatography to TBO. Gibbs free energies were calculated as described above, and values of logK_{ow} were estimated via the Sparc Online Calculator (*29*).

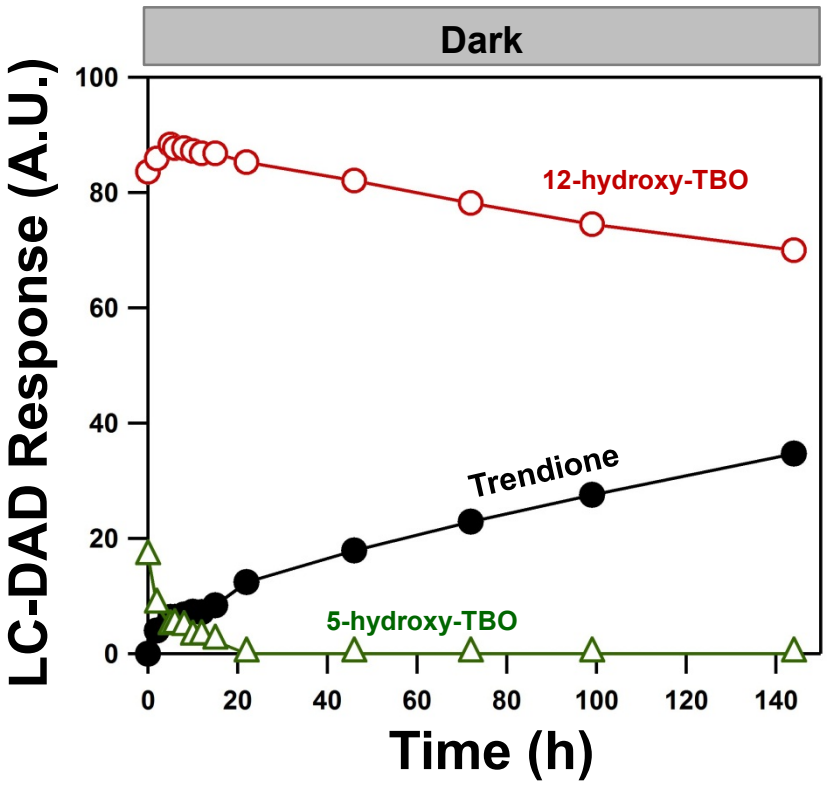

Figure S18.

Dark regrowth of TBO from photoproduct mixtures generated at pH 5 and 25 °C. At pH 5, the minor product (as yet unidentified but believed to be 5-hydroxy-TBO) decays relatively quickly over the first 20 h of dark storage. Over this same time interval, the LC-DAD response associated with the major photoproduct 12-hydroxy-TBO increases. LC-DAD response was measured at 350 nm for TBO and 254 nm for both photoproducts

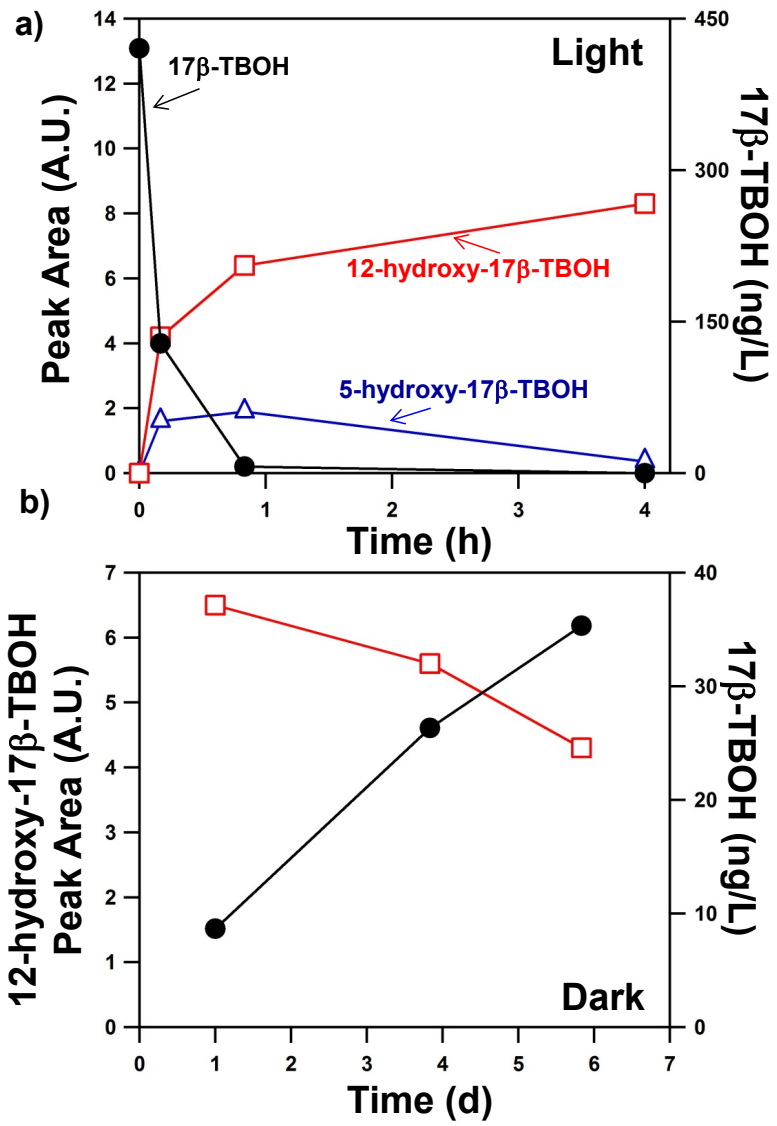

Figure S19.

(a) Concentration profile for 17β-TBOH and its two major photoproducts, 12-hydroxy-17β-TBOH and the presumed 5-hydroxy-17β-TBOH as a function of time during irradiation. Experiments were conducted at an initial 17β-TBOH concentration of 420 ng/L (~1.5 nM) at pH 7. (b) Regrowth of 17β-TBOH (presented as concentration in ng/L on the right y-axis) and decay of 12-hydroxy-17β-TBOH (presented as LC-DAD Peak Area at 254 nm) during the dark storage of the photoproduct mixture generated after the 4 h of irradiation shown in panel (a).

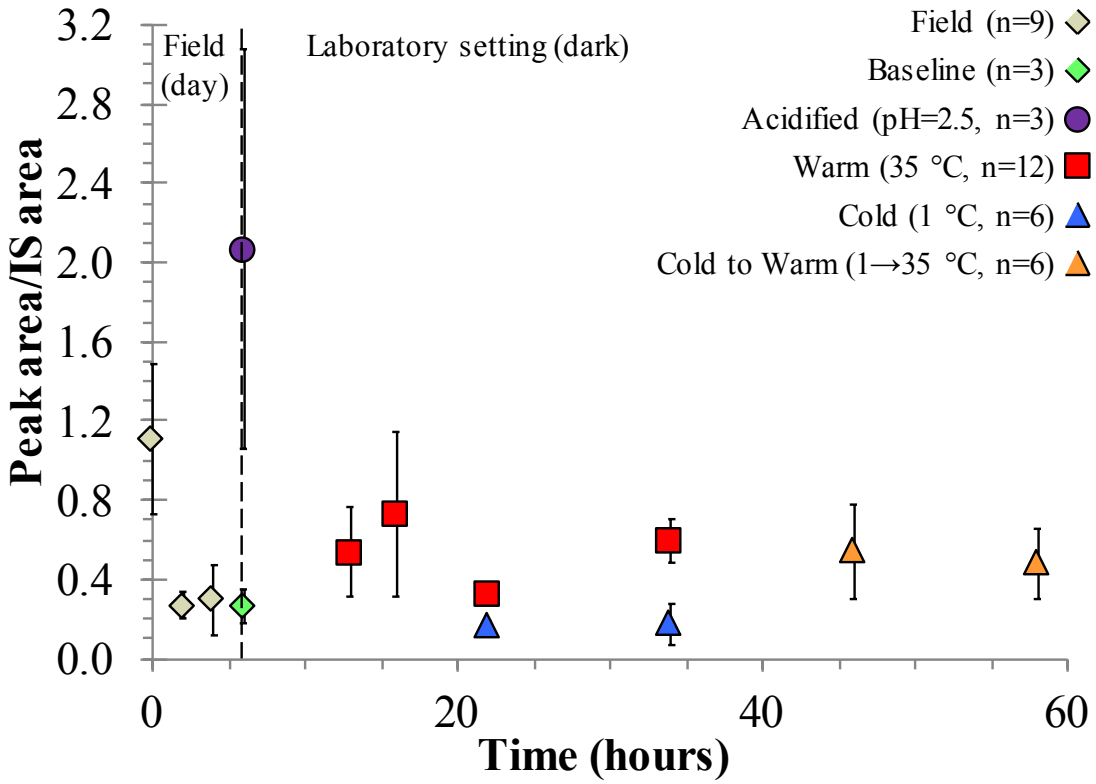

Figure S20.

Peak area responses of a non-target peak, likely steroidal, observed in TBA chromatograms from the field mesocosm samples that exhibits concentration dynamics consistent with those expected for product-to-parent reversion. Additional sample analysis focusing on this non-target peak was performed by examining previously collected mass spectra in samples from a wide range of agricultural receiving waters. This analysis indicated that the non-target peak was present in samples contacted with TBA-implanted manure, was widespread (i.e., occurring in nearly all samples impacted by TBA implantation), and was not present in background samples.

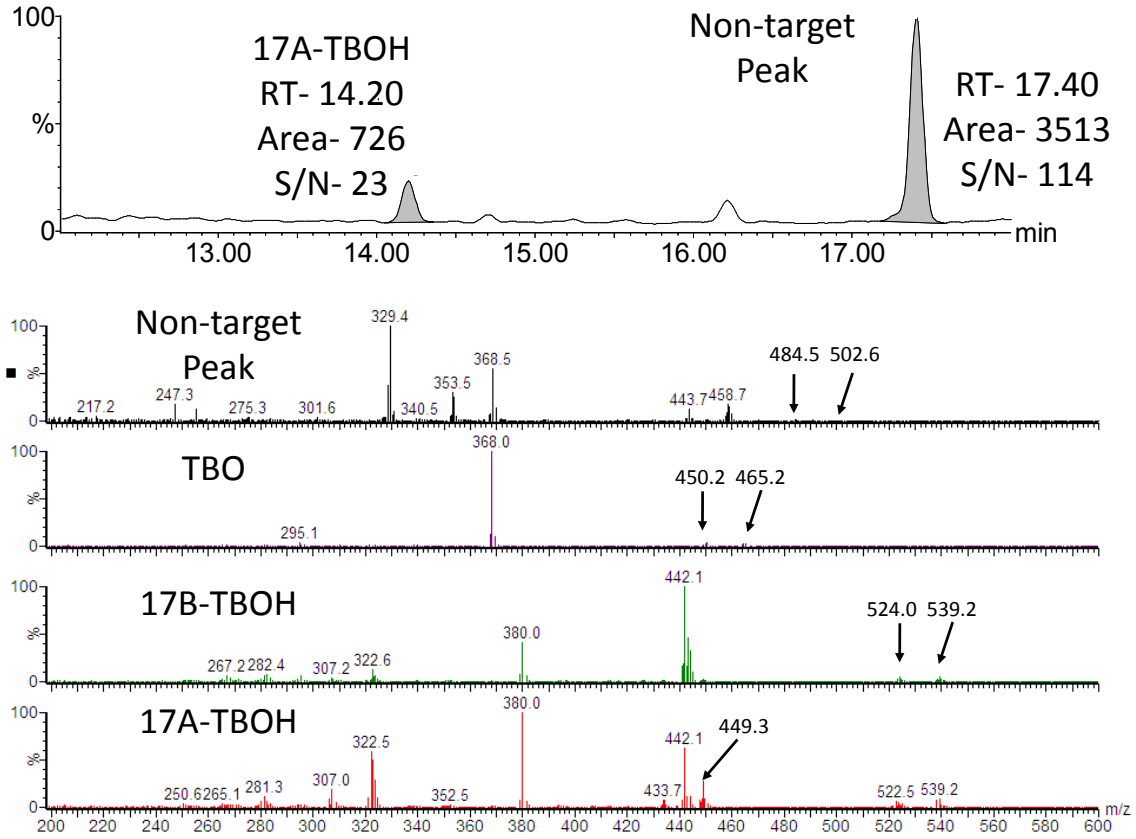

Figure S21.

Gas chromatography-tandem mass spectrometry (GC-MS/MS) chromatogram and spectra of the non-target peak detected in the field mesocosm experiments. The non-target compound peak was initially evident in the MS/MS transitions used to quantify 17α-TBOH. Although this analysis is not definitive and we have not elucidated its structure, full scan and MS/MS spectra are consistent with the non-target species possessing structural similarity to known TBA metabolites, likely containing a conjugated dienone or trienone bond system susceptible to reversible photohydration. Unfortunately, the concentration of this non-target peak (believed to be on the order of 10-100+ ng/L assuming identical peak area response to 17α-TBOH) within agricultural receiving waters remains insufficient to enable structural elucidation via NMR.

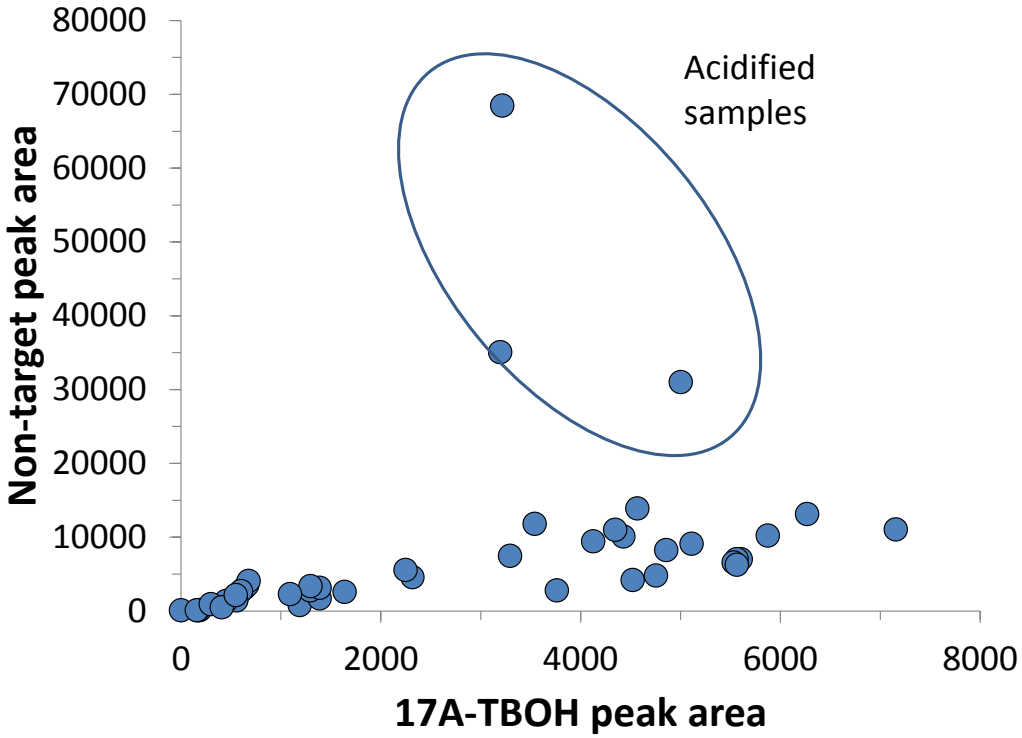

Figure S22.

Scatter plot of the 17α-TBOH and non-target compound peak areas detected in the field mesocosm using the *m/z* 449→323 quantification transition indicating that the occurrence of this non-target peak was highly correlated (using Spearman's rank correlation ($s_r(43) = 0.82$, $p < 0.001$) test) to 17α-TBOH in the field mesocosms. If acidified samples were removed from the analysis (circled samples), the peak areas were still highly correlated using Spearman's rank correlations ($s_r(40) = 0.87$, $p < 0.001$). Based on the Shapiro-Wilk test, the 17α-TBOH concentration and the normalized "non-target metabolite" peak response were not normally distributed ($p<0.01$ for both); therefore, we used Spearman's rank correlation to evaluate the association between 17α-TBOH and the non-target compound.

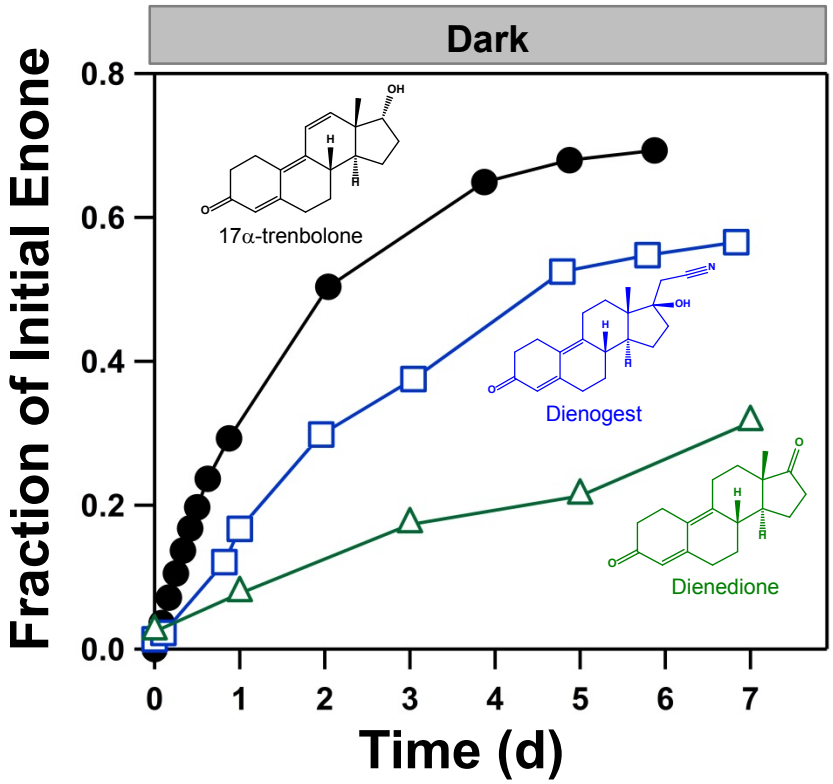

Figure S23.

Reversible photohydration of dienogest, a progestin used as an oral contraceptive (marketed commercially in *Natazia*®) and dienedione, a Schedule III anabolic steroid under the United States Controlled Substances Act that is often illicitly used as a bodybuilding supplement. Upon irradiation with simulated sunlight (at pH 7, 25°C), both dienogest and dienedione underwent rapid (<10 min), near complete photolysis to levels below our limit of analytical detection. Storage of the resulting photoproduct solution in the dark resulted in regrowth of dienogest and dienedione, albeit at rates that are less than that observed for 17α-TBOH (data provided for comparison). This result reveals that reversible photohydration is not just limited to trienone steroids, but also behavior more broadly observable for structurally related steroids (e.g., dienones).

Additional Data Table S1 (separate file).

Data for 17α-TBOH diurnal cycling experiment, results of which are shown in Figure 1a.

Additional Data Table S2 (separate file).

Data for 17α-TBOH, 17β-TBOH, and TBO diurnal cycling experiments, results of which are shown in Figure 1b. Values in red indicate those below our analytical detection limit (see Figure 1 caption for further details)

Additional Data Table S3 (separate file).

Data for the long-term dark reversion of 17α-TBOH, 17β-TBOH, and TBO, which are shown in Figure 2a. Data in italics indicate those collected during photolysis experiments.

Additional Data Table S4 (separate file).

Data for the pH-dependent reversion of 17α-TBOH, which are shown in Figure 2b. Data are only shown for dark regrowth, where C/C_0 values at $t = 0$ have been adjusted to 0 by correcting for any residual 17α-TBOH in solution at the conclusion of the photolysis experiment.

Additional Data Table S5 (separate file).

Data for the temperature-dependent reversion of 17α-TBOH, which are shown in Figure 2c. Data are only provided for the dark regrowth portion of Figure 2c. Photolysis resulted in an initial C/C_0 value of 1 dropping to essentially zero after roughly 4.5 h of irradiation, after which dark regrowth of 17α-TBOH was monitored for approximately 60 h.

Additional Data Table S6 (separate file).

Data for reversion of 17α-TBOH in more complex aquatic matrices, which are shown in the inset of Figure 4. Data are shown for reversion in Iowa River water (IR), as well as solutions of 10 mg/L Fluka Humic Acid (FHA), 5 mM bicarbonate (C), and our model 5 mM phosphate buffer (PB). More details of these matrices are provided in the caption of Figure 4 of the main text.

Additional Data Table S7 (separate file).

Observed concentrations of 17α-TBOH and a non-target peak response (area/17β-TBOH-d3 internal standard area: Area/IS Area) under varying field and laboratory conditions. Background samples were taken from a small collection pond at 22:00 on 7-Dec-2012. No 17α-TBOH was detected (n.d.). The pond was dosed with manure from TBA-implanted heifers at 22:01. On 8-Dec, the pond was in direct sunlight from 08:00-15:00. Samples collected between 22:00 and 15:00 were immediately processed in the field. At 15:00, a 31 L homogeneous "baseline" sample was collected and split into subsamples. A subsample was immediately acidified in the field with 12 M H2SO4 and taken to the laboratory for processing. Upon arrival to the laboratory (19:00, 8-Dec), the baseline sample was further split into subsamples, which were immediately heated ("warm"), refrigerated, ("cold"), or refrigerated and subsequently heated (cold to warm) at 35, 1, or 1→35 °C. Cold to warm samples were placed in an oven at 19:00 on 9-Dec. All

analyzed samples were 1L. Two samples were spiked with 17α-TBOH for recovery analysis. Confidence intervals are indicated as CI.

Additional Data Table S8 (separate file).

Data for 17β-TBOH diurnal cycling experiment, results of which are shown in Figure S11a. Values of 0 (in red) indicate instances where 17β-TBOH was below our analytical limit of detection via LC-DAD.

Additional Data Table S9 (separate file).

Data for TBO diurnal cycling experiment, results of which are shown in Figure S11b. Values of 0 (in red) indicate instances where TBO was below our analytical limit of detection via LC-DAD.

Additional Data Table S10 (separate file).

Data for the semi-log plot of 17α-TBOH concentration as a function of time during irradiation at pH 5 and 7, which are shown in Fig. S12.

Additional Data Table S11 (separate file).

Raw data for species included in Figure S17, optimized at the M06-2X/6-31+G(d,p) level in the presence of SMD water. SMD aqueous solvation was used in all geometry optimizations, hessian calculations and single-point calculations.

Additional Data Table S12 (separate file).

Coordinates for species included in Figure S17, optimized at the M06-2X/6-31+G(d,p) level in the presence of SMD water.

Additional Data Table S13 (separate file).

Data for the dark regrowth of TBO at pH 5, during which interconversion between (presumed) 5-hydroxy TBO (5-OH-TBO) and 12-hydroxy TBO (12-OH-TBO) is proposed to occur. These data are shown in Fig. S18.

Additional Data Table S14 (separate file).

Data for the photolysis and dark regrowth of 17β-TBOH at an environmentally relevant initial concentration (420 ng/L) at pH 7, 25 °C, which are shown in Figure S-19.

Additional Data Table S15 (separate file).

Data for the dark regrowth of 17α-TBOH, dienogest (DG), and dienedione (DD) in dark photoproduct mixtures (pH 7, 25 °C), which are shown in Fig. S-23.

References and Notes

1. K. A. Kidd, P. J. Blanchfield, K. H. Mills, V. P. Palace, R. E. Evans, J. M. Lazorchak, R. W. Flick, Collapse of a fish population after exposure to a synthetic estrogen. *Proc. Natl. Acad. Sci. U.S.A.* **104**, 8897–8901 (2007). doi:10.1073/pnas.0609568104 Medline

2. L. J. Guilette, M. P. Gunderson, Alterations in development of reproductive and endocrine systems of wildlife populations exposed to endocrine-disrupting contaminants. *Reproduction* **122**, 857–864 (2001).. doi:10.1530/rep.0.1220857

3. E. R. Long, D. D. Macdonald, S. L. Smith, F. D. Calder, Incidence of adverse biological effects within ranges of chemical concentrations in marine and estuarine sediments. *Environ. Manage.* **19**, 81–97 (1995). doi:10.1007/BF02472006

4. D. E. Latch, J. L. Packer, W. A. Arnold, K. McNeill, Photochemical conversion of triclosan to 2,8-dichlorodibenzo-p-dioxin in aqueous solution. *J. Photochem. Photobio. A* **158**, 63–66 (2003). doi:10.1016/S1010-6030(03)00103-5

5. K. Fenner, S. Canonica, L. P. Wackett, M. Elsner, Evaluating pesticide degradation in the environment: blind spots and emerging opportunities. *Science* **341**, 752–758 (2013). doi:10.1126/science.1236281 Medline

6. B. Schiffer, A. Daxenberger, K. Meyer, H. H. Meyer, The fate of trenbolone acetate and melengestrol acetate after application as growth promoters in cattle: environmental studies. *Environ. Health Perspect.* **109**, 1145–1151 (2001). doi:10.1289/ehp.011091145 Medline

7. G. T. Ankley, K. M. Jensen, E. A. Makynen, M. D. Kahl, J. J. Korte, M. W. Hornung, T. R. Henry, J. S. Denny, R. L. Leino, V. S. Wilson, M. C. Cardon, P. C. Hartig, L. E. Gray, Effects of the androgenic growth promoter 17-beta-trenbolone on fecundity and reproductive endocrinology of the fathead minnow. *Environ. Toxicol. Chem.* **22**, 1350–1360 (2003). doi:10.1002/etc.5620220623 Medline

8. J. D. Lawrence, M. A. Ibarburu, In *Proceedings of the NCCC-134 Conference on Applied Commodity Price Analysis, Forecasting, and Market Risk Management*. Chicago, IL, 2007.

9. E. J. Durhan, C. S. Lambright, E. A. Makynen, J. Lazorchak, P. C. Hartig, V. S. Wilson, L. E. Gray, G. T. Ankley, Identification of metabolites of trenbolone acetate in androgenic runoff from a beef feedlot. *Environ. Health Perspect.* **114**, (Suppl 1), 65–68 (2006). doi:10.1289/ehp.8055 Medline

10. H. E. Gall, S. A. Sassman, L. S. Lee, C. T. Jafvert, Hormone discharges from a midwest tile-drained agroecosystem receiving animal wastes. *Environ. Sci. Technol.* **45**, 8755–8764 (2011). doi:10.1021/es2011435 Medline

11. K. M. Jensen, E. A. Makynen, M. D. Kahl, G. T. Ankley, Effects of the feedlot contaminant 17alpha-trenbolone on reproductive endocrinology of the fathead minnow. *Environ. Sci. Technol.* **40**, 3112–3117 (2006). doi:10.1021/es052174s Medline

12. Syntex Animal Health, “Synovex Plus (Trenbolone Acetate and Estradiol Benzoate) Implant Environmental Assessment” (1995).

13. D. G. Cornell, E. Avram, N. Filipescu, Photohydration of testosterone and 4-androstene-3,17-dione in aqueous solution. *Steroids* **33**, 485–494 (1979). doi:10.1016/0039-128X(79)90031-X Medline

14. S. Qu, E. P. Kolodziej, D. M. Cwiertny, Phototransformation rates and mechanisms for synthetic hormone growth promoters used in animal agriculture. *Environ. Sci. Technol.* **46**, 13202–13211 (2012). doi:10.1021/es303091c Medline

15. E. P. Kolodziej, S. Qu, K. L. Forsgren, S. A. Long, J. B. Gloer, G. D. Jones, D. Schlenk, J. Baltrusaitis, D. M. Cwiertny, Identification and environmental implications of photo-transformation products of trenbolone acetate metabolites. *Environ. Sci. Technol.* **47**, 5031–5041 (2013). doi:10.1021/es3052069 Medline

16. Materials and methods are available on *Science* Online.

17. R. De Marco, A. Leggio, A. Liguori, F. Perri, C. Siciliano, Transformations of 3-hydroxy steroids with lewis and anhydrous protic acids: the case of pregn-4-en-3β,17α,20β-triol. *Chem. Biol. Drug Des.* **78**, 269–276 (2011). doi:10.1111/j.1747-0285.2011.01147.x Medline

18. K. R. Stackhouse, C. A. Rotz, J. W. Oltjen, F. M. Mitloehner, Growth-promoting technologies decrease the carbon footprint, ammonia emissions, and costs of California beef production systems. *J. Anim. Sci.* **90**, 4656–4665 (2012). doi:10.2527/jas.2011-4654 Medline

19. V. S. Blazer, L. R. Iwanowicz, H. Henderson, P. M. Mazik, J. A. Jenkins, D. A. Alvarez, J. A. Young, Reproductive endocrine disruption in smallmouth bass (Micropterus dolomieu) in the Potomac River basin: spatial and temporal comparisons of biological effects. *Environ. Monit. Assess.* **184**, 4309–4334 (2012). doi:10.1007/s10661-011-2266-5 Medline

20. J. K. Leet, L. S. Lee, H. E. Gall, R. R. Goforth, S. Sassman, D. A. Gordon, J. M. Lazorchak, M. E. Smith, C. T. Javfert, M. S. Sepúlveda, Assessing impacts of land-applied manure from concentrated animal feeding operations on fish populations and communities. *Environ. Sci. Technol.* **46**, 13440–13447 (2012). doi:10.1021/es302599t Medline

21. D. A. Stavreva *et al.*, *Sci. Rep.* **2**, (2012).

22. M. Oettel, A. Kurischko, STS 557, a new orally active progestin with antiprogestational and contragestational properties in rabbits. *Contraception* **21**, 61–75 (1980). doi:10.1016/0010-7824(80)90140-7 Medline

23. Y. Zhao, D. Truhlar, The M06 suite of density functionals for main group thermochemistry, thermochemical kinetics, noncovalent interactions, excited states, and transition elements: two new functionals and systematic testing of four M06-class functionals and 12 other functionals. *Theor. Chem. Acc.* **120**, 215–241 (2008). doi:10.1007/s00214-007-0310-x

24. A. V. Marenich, C. J. Cramer, D. G. Truhlar, Universal solvation model based on solute electron density and on a continuum model of the solvent defined by the bulk dielectric constant and atomic surface tensions. *J. Phys. Chem. B* **113**, 6378–6396 (2009). doi:10.1021/jp810292n Medline

25. M. J. Frisch *et al*., Gaussian 09, Version B02. Gaussian, Inc., Wallingford CT, 2009.

26. J. A. Parker, J. P. Webster, S. C. Kover, E. P. Kolodziej, Analysis of trenbolone acetate metabolites and melengestrol in environmental matrices using gas chromatography-tandem mass spectrometry. *Talanta* **99**, 238–246 (2012). doi:10.1016/j.talanta.2012.05.046 Medline

27. J. P. Webster, S. C. Kover, R. J. Bryson, T. Harter, D. S. Mansell, D. L. Sedlak, E. P. Kolodziej, Occurrence of trenbolone acetate metabolites in simulated confined animal feeding operation (CAFO) runoff. *Environ. Sci. Technol.* **46**, 3803–3810 (2012). doi:10.1021/es204529v Medline

28. W. Sadée, S. Riegelman, L. F. Johnson, On the mechanism of steroid fluorescence in sulfuric acid. I. The formation of trienones. *Steroids* **17**, 595–606 (1971). doi:10.1016/S0039-128X(71)80160-5 Medline

29. Sparc Online Calculator, available at http://ibmlc2.chem.uga.edu/sparc/ (accessed May 14, 2013).